II. PLASMA DYNAMICS

A. PLASMA PHYSICS*

Prof. S. C. Brown	Dr. S. Gruber	P. J. Freyheit
Prof. W. P. Allis	Dr. J. L. Hirshfield	R. B. Hall
Prof. D. J. Rose	C. D. Buntschuh	W. R. Kittredge
Prof. D. R. Whitehouse	J. D. Coccoli	J. J. McCarthy
Dr. G. Bekefi	E. W. Fitzgerald	W. J. Mulligan
Dr. B. Brandt	S. Frankenthal	J. J. Nolan, Jr.

1. RADIATION FROM PLASMAS WITH NON-MAXWELLIAN DISTRIBUTIONS

In the interpretation of measurements (1, 2, 3) of the incoherent microwave radiation from plasmas, it is generally assumed that the radiation temperature T_r equals the electron temperature T_e. Here, we investigate departures from this equality when the electrons do not have a Maxwellian velocity distribution.

Consider a plasma in a steady state, in which electrons of concentration n collide with ions or atoms of concentration N. When the steady state is established for both the radiation and the electron gas, the rate of emission of radiation in the frequency interval between ω and $(\omega+d\omega)$ balances the rate of absorption. Incoherent scattering of radiation is neglected here (4, 5).

Let $Q_r(w)$ be the cross section for spontaneous emission of radiation of energy $\hbar\omega$ (for one polarization of the wave) by an electron of velocity w. Let G(w) be the cross section per unit intensity of radiation for stimulated emission, and H(v) be the cross section per unit intensity for stimulated absorption of a photon $\hbar\omega$ by an electron of velocity v. Equating the rate of energy radiated in a given direction with the rate of energy absorbed in that direction, we obtain (for one polarization),

$$\int Nn\, w[Q_r(w)+G(w)B(\omega, T_r)]\, 4\pi\, f(w)\, w^2\, dw\hbar\omega$$

$$= \int Nn\, v\, H(v)\, B(\omega, T_r)\, 4\pi\, f(v)\, v^2\, dv\hbar\omega \qquad (1)$$

where f is the distribution of electron velocities normalized so that $\int_0^\infty f(v)\, 4\pi\, v^2\, dv = 1$, $B(\omega,T_r)$ is the steady-state intensity, and w and v are related by

$$(m/2)[w^2-v^2] = \hbar\omega$$

$$w\, dw = v\, dv \qquad (2)$$

---

*This work was supported in part by the Atomic Energy Commission under Contract AT(30-1)-1842; in part by the Air Force Cambridge Research Center under Contract AF-19(604)-5992; and in part by National Science Foundation under Grant G-9330.

The cross sections are independent of the nature of the steady state that prevails in the radiating medium. Their interrelationship is obtained (6) by assuming f to be a Maxwellian distribution, with T_r equal to the electron temperature $T_e = 2\bar{u}/3k$ (where $\bar{u}$ is the mean electron energy), and with the intensity $B(\omega, T_e)$ per unit radian frequency interval equal to the Planck function, $(\hbar\omega^3/8\pi^3c^2)[\exp(\hbar\omega/kT_e)-1]^{-1}$. Then we have

$$Q_r(w)/H(v) = (\hbar\omega^3/8\pi^3c^2)(v/w)^2$$

and (3)

$$Q_r(w)/G(w) = (\hbar\omega^3/8\pi^3c^2)$$

Substituting Eqs. 2 and 3 in Eq. 1, we obtain

$$B(\omega, T_r) = \frac{\hbar\omega^3}{8\pi^3c^2} \int w^2Q_r(w)\, f(w)\, v\, dv \Big/ \int w^2Q_r(w)[f(v)-f(w)]\, v\, dv \tag{4}$$

Equation 4 gives the black-body radiation intensity of a plasma with an arbitrary distribution of electron velocities f and an arbitrary radiation cross section Q_r. In using Eq. 4, we set $B(\omega, T_r)$ equal to $(\hbar\omega^3/8\pi^3c^2)[\exp(\hbar\omega/kT_r)-1]^{-1}$, and thus define the radiation temperature T_r:

$$[\exp(\hbar\omega/kT_r)-1]^{-1} = \int w^2Q_r(w)\, f(w)\, v\, dv \Big/ \int w^2Q_r(w)[f(v)-f(w)]\, v\, dv \tag{5}$$

When $f(v) = \exp\left(-mv^2/2kT_e\right)$, it can be shown that $T_r = T_e$ for any dependence of Q_r on w. At low frequencies, $\hbar\omega/kT_r \ll 1$, $w \to v$, $f(v) \to f(w) - (\hbar\omega/mv)\, \partial f/\partial v$, and Eq. 5 reduces to

$$kT_r = -m \int_0^\infty Q_r(v)\, f(v)\, v^3\, dv \Big/ \int_0^\infty Q_r(v)\, \frac{\partial f(v)}{\partial v}\, v^2\, dv \tag{6}$$

In applying Eq. 6 to specific cases it is helpful to replace the radiation cross section Q_r by an absorption cross section that can be more easily deduced from measured quantities. In obtaining this absorption cross section, we also indicate how Eq. 6 is derived from the rf conductivity of the plasma.

The intensity of spontaneous emission j_ω is

$$j_\omega = \int Nn\, v Q_r(v)\, 4\pi\, f(v)\, v^2\, dv\hbar\omega \tag{7}$$

The absorption coefficient α_ω for a tenuous plasma of refractive index close to unity and of low absorptivity (assumptions that are implicit throughout these calculations) is related (1) to the real part of the rf conductivity σ_r by

$$a_\omega = \sigma_r/\epsilon_o c \tag{8}$$

where a_ω is the total absorption, that is, the stimulated absorption reduced by the stimulated emission. The conductivity of a low-temperature plasma (7) (with contributions from ion motion neglected) is given by

$$\sigma_r = -\int (4\pi\ Nn\ e^2/3m\omega^2)\ R(v)\frac{\partial f(v)}{\partial v} v^4\ dv \tag{9}$$

where e and m are the electron charge and mass, respectively, and R(v) is an absorption cross section whose exact form depends on frequency and on the presence or absence of external magnetic fields. We shall define R(v) when we treat particular cases. To relate $Q_r(v)$ to R(v), we use Kirchhoff's law, $j_\omega = a_\omega B(\omega, T_r)$, in conjunction with Eqs. 7, 8, and 9. We assume f(v) to be Maxwellian (with $T_r = T_e$), and obtain the relation between Q_r and R(v):

$$Q_r(v) = \left(e^2/24\pi^3 c^3 \epsilon_o\right) R(v)\ v^2\ d\omega/\hbar\omega \tag{10}$$

Substituting Eq. 10 for Q_r in Eq. 7, and setting the ratio j_ω/a_ω equal to $B(\omega, T_r)$, we find that

$$kT_r = -m \int_0^\infty R(v)\ f(v)\ v^5\ dv \Big/ \int_0^\infty R(v)\frac{\partial f(v)}{\partial v} v^4\ dv \tag{11}$$

which is identical with Eq. 6 with R replaced by Q_r.

a. Examples

In making computations from Eq. 11 we shall assume for simplicity, that the distribution function $f = \exp[-b(v/\bar{v})^\ell]$, where b and ℓ are positive constants, and $\bar{v}$ is the mean electron velocity.

(i) Bremsstrahlung

For bremsstrahlung, radiation originates from collisions of electrons with atoms or ions. In this case R(v) is given by

$$R(v) = \frac{\omega^2 Q_m(v)}{\omega^2 + [NvQ_m(v)]^2} \tag{12}$$

where $Q_m(v)$ is the collision cross section for momentum transfer (8). We note that at high frequencies (or at low values of N) R(v) varies proportionally as $Q_m(v)$, while at low frequencies (or at high values of N) R(v) varies as $v^{-2}Q_m^{-1}(v)$.

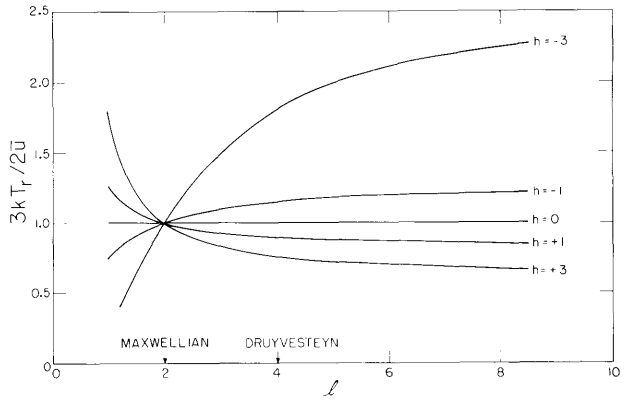

Fig. II-1. Radiation temperature for bremsstrahlung as a function of the distribution of electron velocities; $f(v) \propto \exp[-b(v/\bar{v})]$ and $Q_m(v) = a(v/\bar{v})^{h-1}$.

Figure II-1 shows how the ratio $(3kT_r/2\bar{u})$ varies with the distribution function for different cross sections, $Q_m(v)$. The computations were made in the limit of high frequencies and with the assumption that $Q_m(v) = a(v/\bar{v})^{h-1}$, where a and h are constants. We see that the ratio $(3kT_r/2\bar{u})$ is equal to unity in two cases: when f is Maxwellian, $\ell = 2$; and when $Q_m(v)$ varies inversely as the velocity, h = 0 — that is, when the collisions occur at a constant mean-free time. The departure from unity is greatest for large negative values of h (h = −3 is valid, approximately, in a fully ionized gas).

(ii) Radiation in the Presence of a Magnetic Field

Electrons also radiate as a result of their orbital motion in the magnetic field. The absorption of the wave α_ω depends on θ, the angle between the direction of observation of the radiation and the magnetic field. For purposes of calculation, we assume that only the elliptically polarized wave, whose electric vector rotates with the electrons, contributes significantly to α_ω. This limits the calculations to frequencies not far removed from the electron cyclotron frequency, ω_b. The absorption cross section R(v) then becomes (2)

$$R(v) = \frac{\omega^2 Q_m(v)[(1 + \cos^2\theta)/2]}{(\omega-\omega_b)^2 + (NvQ_m(v))^2} \tag{13}$$

The frequency spectrum of R(v) given in Eq. 13 is characteristic of a pressure-broadened Lorentzian line. Equation 13 neglects Doppler shift of the radiation that results from the thermal motion of the electrons, and it also neglects the higher harmonics of the cyclotron radiation (9). Integrals that result from a substitution of Eq. 13 in Eq. 11 were evaluated with the aid of functions tabulated by Dingle, Arndt, and Roy (10).

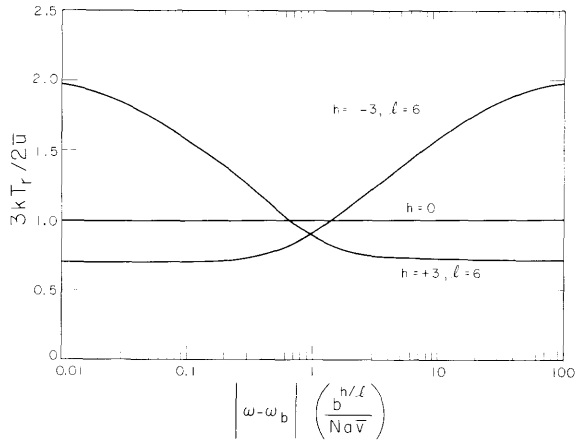

Fig. II-2. Radiation temperature for cyclotron radiation as a function of frequency (pressure broadening).

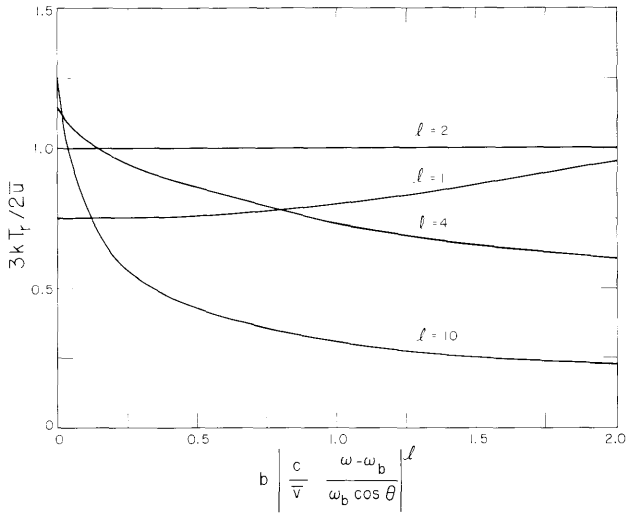

Fig. II-3. Radiation temperature as a function of frequency for cyclotron radiation (Doppler broadening).

Figure II-2 shows a plot of $(3kT_r/2u)$ as a function of frequency. As in Fig. II-1, large departures of the radiation temperature T_r from the electron temperature T_e occur for h = -3.

When thermal motion of the electrons becomes important (Doppler effect), Eq. 13 has the form

$$R(v) = \frac{\omega^2 Q_m(v)[(1 + \cos^2\theta)/2]}{[\omega - \omega_b(1 - (v/c)\cos\phi\cos\theta)]^2 + [NvQ_m(v)]^2} \tag{14}$$

where ϕ is the angle between the directions of v and the magnetic field. In making calculations of T_r from Eqs. 11 and 14, the volume element $d^3v = 4\pi v^2 dv$ of Eq. 11 must be replaced by the volume element, $d^3v = 2\pi v^2 dv \sin\phi\, d\phi$, and the integrands of Eq. 11 must be integrated over ϕ from 0 to 2π. In the limit of zero collision frequency (i.e., $\langle NvQ_m(v)\rangle \to 0$), and for θ not equal to $\pi/2$, we obtain the radiation temperature for Doppler broadening only:

$$kT_r = -m \int_\Delta^\infty f(v)\, v^3\, dv \Big/ \int_\Delta^\infty \frac{\partial f(v)}{\partial v}\, v^2\, dv \tag{15}$$

where $\Delta = c|(\omega-\omega_b)|/\omega_b \cos\theta$. Use of the distribution functions of the form $f(v) = \exp[-b(v/v)^\ell]$ leads to solutions of Eq. 15 in terms of incomplete gamma functions (11).

Figure II-3 illustrates how T_r varies with frequency in the vicinity of $\omega = \omega_b$.

(iii) Negative Radiation Temperatures

A system in which stimulated emission exceeds stimulated absorption exhibits a negative total absorption α_ω (Eqs. 8 and 9), and thus, by Kirchhoff's law, has a negative radiation temperature (12). In this case the radiation intensity can greatly exceed the intensity from a system that has a positive temperature because in this instance, the electromagnetic waves generated at some point within the medium are amplified in traversing the medium.

Equation 11 can be used to establish conditions for negative temperatures in plasmas, at microwave frequencies. Since R(v) and f(v) are positive quantities, T_r can be negative only if $\partial f(v)/\partial v > 0$ over some range of electron velocity. In other words; in some region of velocity space, there must be an excess of energetic electrons, as compared with the population in neighboring regions. Although this is a necessary condition, the attainment of a negative temperature depends on the precise variation of R(v) with v. A second necessary condition is obtained by integrating by parts the denominator D of Eq. 11. Since $f(\infty) = 0$,

$$D = -f(0)[R(v)v^4]_{v=0} - \int_0^\infty f(v)\, \frac{\partial}{\partial v}\, [R(v)v^4]\, dv \tag{16}$$

from which it follows, that T_r can be negative only if $d[R(v)v^4]/dv < 0$, over some finite region of electron velocity.

Criteria similar to these were given by Twiss (5), who applied them to several specific radiation processes.

G. Bekefi, J. H. Hirshfield

References

1. G. Bekefi, J. L. Hirshfield, and S. C. Brown, Phys. Rev. 116, 1051 (1959).

2. J. L. Hirshfield and S. C. Brown, Incoherent microwave radiation from plasmas in magnetic fields (submitted for publication to Phys. Rev.).

3. G. Bekefi and S. C. Brown, Microwave measurements of the radiation temperature of plasmas (submitted for publication to J. Appl. Phys.).

4. A. V. Phelps and A. O. McCoubrey, Phys. Rev. 118, 1561 (1960).

5. R. Q. Twiss, Australian J. Phys. 11, 564 (1958).

6. G. Cillié, Monthly Notices Roy. Astron. Soc. 92, 820 (1932).

7. W. P. Allis, Motions of electrons and ions, Handbuch der Physik, Vol. 21 (Springer Verlag, Berlin, 1956), pp. 383-444.

8. S. C. Brown, Basic Data of Plasma Physics (Technology Press of Massachusetts Institute of Technology, Cambridge, Mass., and John Wiley and Sons, Inc., New York, 1959).

9. J. L. Hirshfield and S. C. Brown, Cyclotron radiation from a hot plasma (submitted for publication to Phys. Fluids).

10. R. B. Dingle, D. Arndt, and S. K. Roy, Appl. Sci. Research B6, 144-164 (1957).

11. K. Pearson, Tables of the Incomplete Gamma-Function (H. M. Stationery Office, London, 1922).

12. C. Kittel, Elementary Statistical Physics (John Wiley and Sons, Inc., New York, 1958).

2. CESIUM VAPOR TECHNIQUES IN THE PRODUCTION OF FULLY IONIZED PLASMAS

Because of the need for a fairly long fully-ionized plasma column with which to experiment and because of the difficulties with the cesium beam methods previously used (1), the use of cesium vapor for plasma production was attempted. This method is similar to the use of mercury vapor in the production of gas discharges; however, all ionization is done, as with the beam techniques, by contact with a hot tungsten surface. The tube constructed is shown schematically in Fig. II-4.

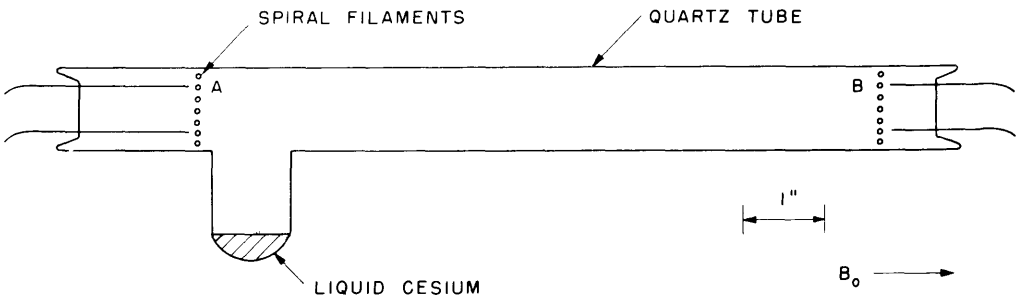

Fig. II-4. Cesium-vapor tube.

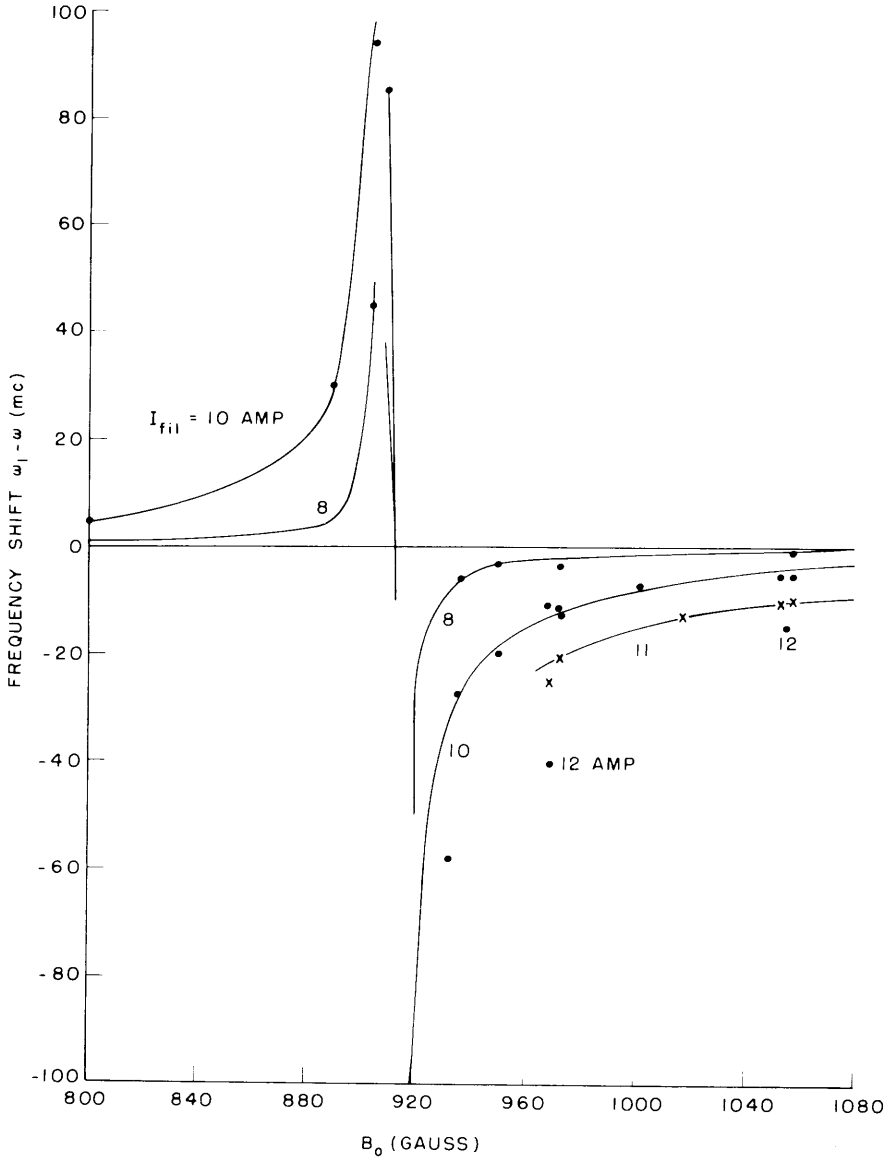

Fig. II-5. Frequency shift of room-temperature cesium plasma.

Filaments A and B are flat tungsten spiral filaments of 5/8 inch diameter. The liquid cesium in the side arm is obtained by condensing the liquid cesium from capsules contained in another side arm which has been sealed off under vacuum.

Electron-density measurements on this tube were attempted by using a TM_{020} mode cylindrical cavity with the electric field parallel to the dc magnetic field. At two different cesium vapor pressures (dry ice and acetone temperature, and room temperature) these measurements were found to be impossible. As soon as the temperature of the tungsten filaments was brought to a high value the cavity Q would steadily decrease until

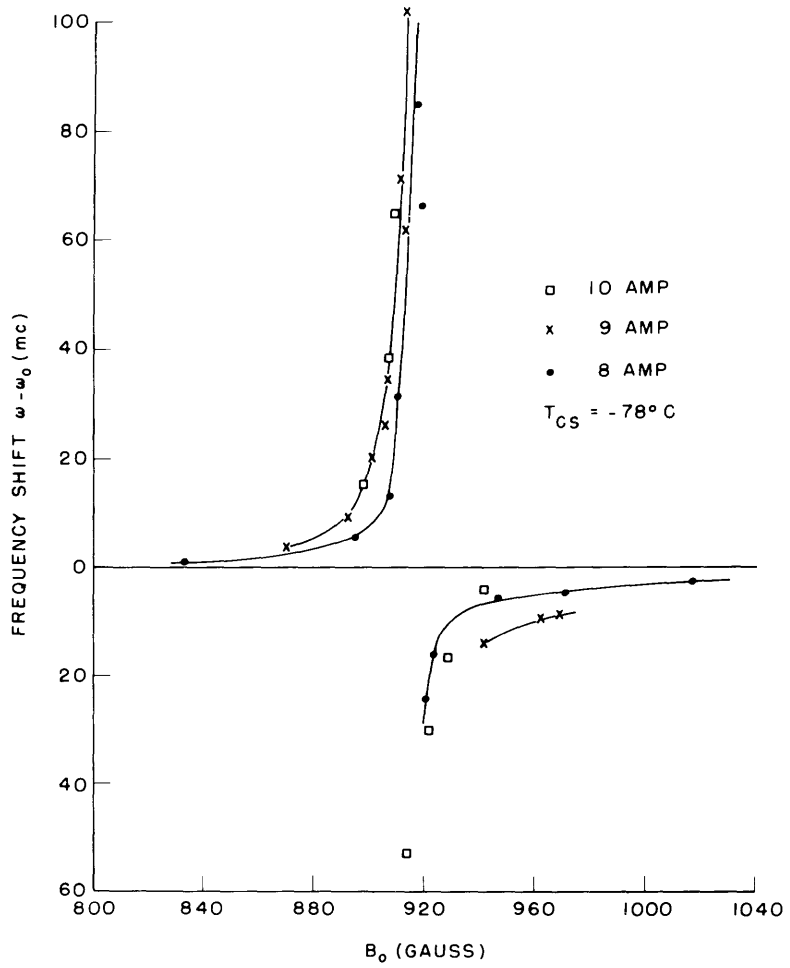

Fig. II-6. Frequency shift of −77°C cesium plasma versus magnetic field.

the absorption could not be found. As a result, no measurements were obtained with the use of this cavity.

In place of the TM_{020} cavity, a TM_{010} mode cavity with the electric field transverse to the dc magnetic field was used for measurement of the electron density. The second cavity did not suffer the malady of the longitudinal-field cavity and density measurements were obtained. Figure II-5 shows the frequency shift of the cavity plotted versus the dc magnetic field. These curves, at room-temperature cesium vapor pressure, indicate that there are insufficient electrons for every ion produced on the hot tungsten surface to produce complete space-charge neutralization. This is seen from the fact that the density continues to increase as the filament current is increased.

Frequency-shift curves with the cesium at −77°C were also obtained and are shown in Fig. II-6. In contrast to the room-temperature results, increasing the filament temperature does very little to increase the electron density because much fewer neutral

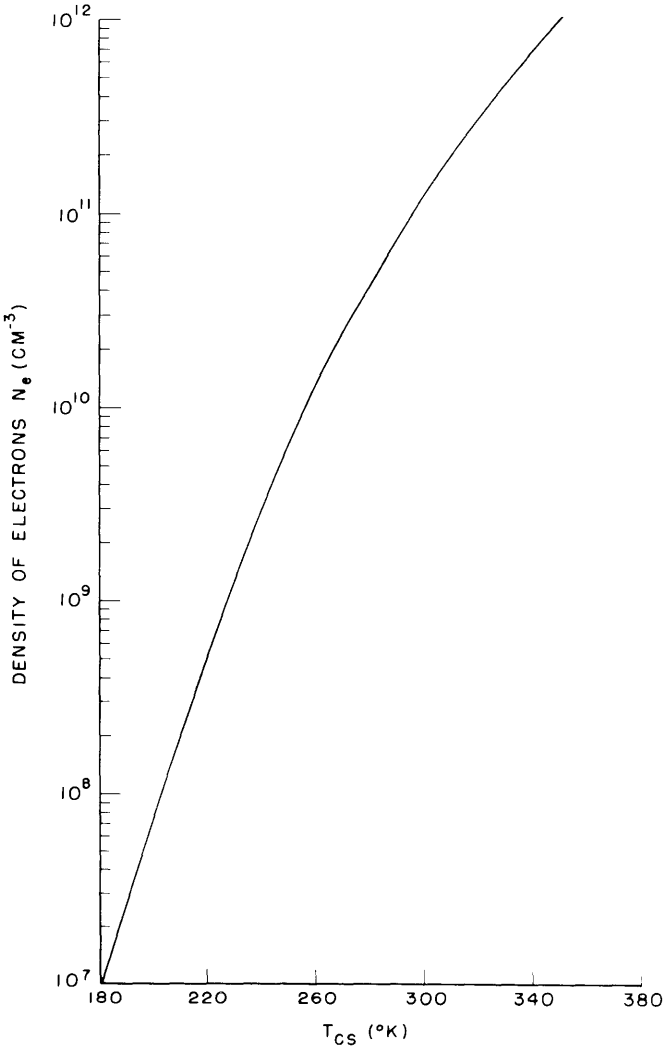

Fig. II-7. Recombination-limited electron density versus T_{Cs}. Plasma length, 13 inches; $\alpha = 3.4 \times 10^{-10}$ cm^3 T^{-1}.

cesium atoms are available for ionization on the hot tungsten surfaces.

Calculation of the electron density from the frequency shift and the known magnetic field yields an approximate density of

$$N_e = 8 \times 10^8 \text{ electrons/cc} \quad (1)$$

at T_{Cs} = 293°K and I = 12 amp, and

$$N_e = 8 \times 10^7 \text{ electrons/cc} \quad (2)$$

at T_{Cs} = 200°K.

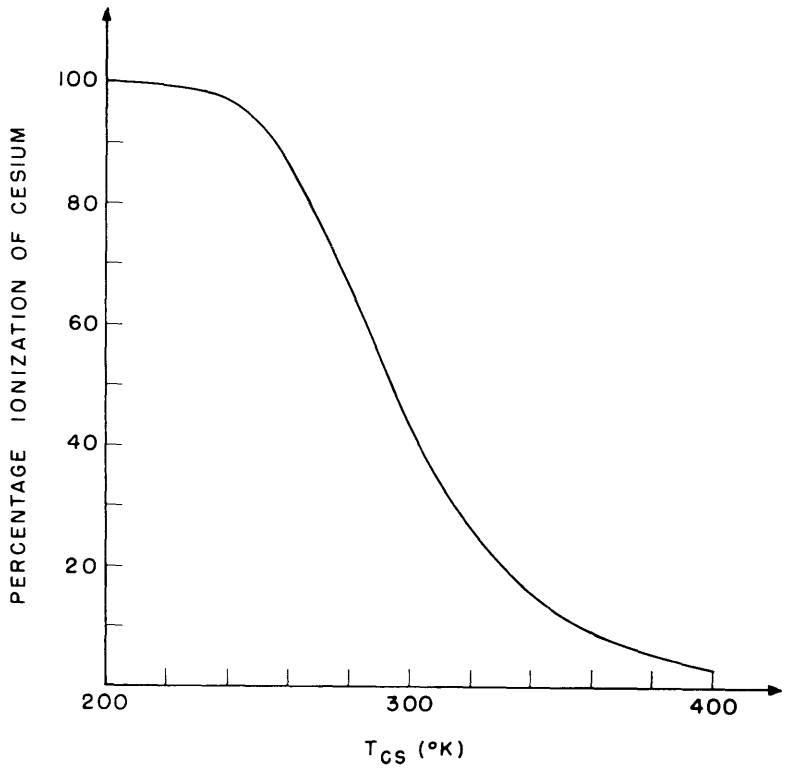

Fig. II-8. Percentage of ionization of cesium versus temperature of cesium.

The electron densities given in Eqs. 1 and 2 are quite low, and one wonders what the fundamental limitations on achieving high densities are. Presumably, there can be no diffusion caused by ion-atom collisions, since the mean-free path (2) at a temperature of 300°K is of the order of magnitude of 10 meters. Another loss mechanism that can be examined is that caused by electron-ion radiative recombination. Thus, in order to find the electron-density limitations, the total loss is assumed to be due only to recombination, and the production rate is assumed to be limited only by the arrival rate of neutral cesium on the hot tungsten filaments. The total loss of ions per second is, then,

$$\frac{dN_i}{dt} = \alpha N_i^2 V \tag{3}$$

where α is the recombination coefficient, and V is the total volume of plasma. Equation 3 is set equal to the arrival rate u_a of neutral cesium atoms (2) which is dependent on the temperature of cesium, T_{Cs}. We then obtain

$$\alpha N_i^2 L = u_a \tag{4}$$

where L is the plasma column length. Using the recombination coefficient (3),

$$\alpha = 3.4 \times 10^{-10} (\text{cm}^3\ \text{sec}^{-1}) \tag{5}$$

and the tube length of 13 inches we can obtain the curve of maximum electron density versus cesium pressure shown in Fig. II-7.

Comparison of Fig. II-7 with the experimental measurements given by Eqs. 1 and 2 shows that the conclusions reached about the loss mechanisms are valid. At 200°K the recombination limited density is indeed what we measure. On the other hand, at room temperature we find a maximum possible electron density nearly two orders of magnitude greater than the measured order of magnitude. This again supports our general conclusion that not enough electrons are being thermionically emitted to neutralize the space charge of all produced ions. This deficit should be corrected by increasing the filament current.

We have, thus far, not discussed what percentage of ionization is obtainable with the cesium-vapor tube. The percentage of ionization versus T_{Cs} is plotted in Fig. II-8; here we have used Fig. II-7 and the arrival rate u_a in the calculation. It can be observed that one can never obtain a high-density fully ionized plasma with the use of a cesium-vapor tube; however, one can obtain, for example, 50 per cent ionization at a density of nearly 10^{11} electrons/cc.

Since, generally speaking, a considerable amount of useful experimentation on the properties of fully ionized plasmas can be obtained with even 50 per cent ionization, the further usefulness of the cesium-vapor tube seems to be evident, and, because of its relative simplicity, it should provide a convenient source with which to work.

R. B. Hall, B. Brandt

References

1. R. B. Hall and G. Bekefi, Cesium plasma, Quarterly Progress Report No. 55, Research Laboratory of Electronics, M.I.T., Oct. 15, 1959, p. 16; No. 56, Jan. 15, 1960, p. 20.

2. W. B. Nottingham, Cesium plasma diode as heat to electrical power transducer, Internal Memorandum, Research Laboratory of Electronics, M.I.T., 1959.

3. S. C. Brown, Basic Data of Plasma Physics (Technology Press of Massachusetts Institute of Technology, Cambridge, Mass., and John Wiley and Sons, Inc., New York, 1959), p. 195.

II-B. PLASMA ELECTRONICS*

Prof. L. D. Smullin
Prof. H. A. Haus
Prof. A. Bers
Prof. D. J. Rose
P. Chorney
L. J. Donadieu
T. H. Dupree
T. J. Fessenden
W. D. Getty
L. M. Lidsky
A. Peskoff
S. D. Rothleder
R. C. Wingerson
S. Yoshikawa

1. THERMAL NOISE FROM PLASMAS

Thermal noise radiated by a plasma at a uniform temperature can be evaluated if the absorption characteristics of the plasma are known (1, 2). This method fails when the plasma is not at a uniform temperature. When the deviation of the distribution functions of the charge carriers from the equilibrium distribution is small, and this includes all cases for which a temperature can be reasonably defined, we would expect that the radiated noise power can be computed as the superposition of the noise powers radiated from the various volume elements of the plasma, each element at a particular temperature radiating the noise power it would radiate at equilibrium if kept at the same temperature. Such an analysis calls for an approach to the fluctuation problem that considers each differential volume element separately as an absorber and emitter of noise power. It calls for the introduction into Maxwell's equations of a source term that is analogous to the source terms in the Langevin equation in the theory of Brownian motion (3). The main problem is, then, the determination of the time- and space-correlation functions of the source term. Aside from their use in problems involving radiation from plasmas, the correlation functions can give helpful insight into the fluctuation processes.

As a first step toward the solution of the complete problem, the correlation functions of the source term have been determined for a uniform plasma, with the use of thermodynamic considerations. The method is applicable to any uniform linear medium for which the relation between the electric field and driven-current density $\bar{J}_d$ can be written in the form

$$\bar{J}_d = \bar{\bar{D}} \cdot \bar{E} \tag{1}$$

where $\bar{\bar{D}}$ is a linear tensor operator in the time and space variables. Maxwell's equations can be written in the form

$$\nabla \times \bar{E} = -\mu_o \frac{\partial \bar{H}}{\partial t} \tag{2}$$

$$\nabla \times \bar{H} = \epsilon_o \frac{\partial \bar{E}}{\partial t} + \bar{\bar{D}} \cdot \bar{E} + \bar{K} \tag{3}$$

where $\bar{K}$ is the source current density. We introduce Fourier transforms in time

*This work was supported in part by National Science Foundation under Grant G-9330.

through the use of periodic substitute functions defined by, for example,

$$\begin{aligned} &\bar{K}(t, \bar{r}, T) = \bar{K}(t, \bar{r}) \qquad -(T/2) < t < (T/2) \\ &\bar{K}(t+nT, \bar{r}, T) = \bar{K}(t, \bar{r}, T) \end{aligned} \tag{4}$$

The Fourier transform of $\bar{K}(t, \bar{r}, T)$ is $\bar{K}(\omega, \bar{r}, T)$.

It is convenient to imagine the uniform medium enclosed in a very large cubic cavity. The field quantities could be expanded in terms of the normal (solenoidal and divergence) modes of the cavity in the usual way. Here, we use modes satisfying periodic boundary conditions (traveling waves). Furthermore, we do not separate the modes into solenoidal and divergence modes but use modes that have both a divergence and a curl. We comprise in one "mode," characterized by a propagation vector $\bar{k}$, the three vector functions

$$\bar{i}_x e^{-j\bar{k}\cdot\bar{r}}, \quad \bar{i}_y e^{-j\bar{k}\cdot\bar{r}}, \quad \bar{i}_z e^{-j\bar{k}\cdot\bar{r}}$$

The propagation vector $\bar{k}$ assumes the values

$$\bar{k} = \frac{2\pi m}{L}\bar{i}_x + \frac{2\pi n}{L}\bar{i}_y + \frac{2\pi p}{L}\bar{i}_z \tag{5}$$

where m, n, and p are integers, and L is the linear dimension of the cube. In the limit $L \to \infty$ the propagation constant may assume a continuous range of values.

Now let us consider any field quantity, say $\bar{K}(\omega, \bar{r}, T)$. When expanded in terms of the normal modes it becomes

$$\bar{K}(\omega, \bar{r}, T) = \sum_{k} \bar{K}(\omega, \bar{k}, T, L)\, e^{-j\bar{k}\cdot\bar{r}} \tag{6}$$

where

$$\bar{K}(\omega, \bar{k}, T, L) = \frac{1}{L^3}\int \bar{K}(\omega, \bar{r}, T)\, e^{j\bar{k}\cdot\bar{r}}\, d\bar{r}$$

Introducing these expansions into Maxwell's equations, and omitting the reference to the variables $(\omega, \bar{k}, T, L)$, we obtain

$$-j\bar{k} \times \bar{E} = -j\omega\mu_o \bar{H} \tag{7}$$

$$-j\bar{k} \times \bar{H} = j\omega\epsilon_o \bar{E} + \bar{\bar{D}} \cdot \bar{E} + \bar{K} \tag{8}$$

where $\bar{\bar{D}}$ is now a tensor with components that are algebraic functions of ω and $\bar{k}$.

Equations 7 and 8 may be written in a form that leads directly to an equivalent circuit for the amplitude of each mode. We set $\frac{j\omega\epsilon_o}{|\bar{k}|} \to j\omega C$. We replace the two following square tensors by matrices of third order:

$$\frac{1}{|\bar{k}|}\,\bar{\bar{D}}(\omega, \bar{k}) \rightarrow Y_{ij}$$

$$\frac{1}{j\omega\mu_o|\bar{k}|}\left[\bar{k}^2\,\bar{\bar{I}} - \bar{k}\bar{k}\right] \rightarrow Z_{ij}^{-1}$$

with i, j = x, y, z. We replace the vectors by column matrices of third order:

$$L^{3/2}\frac{1}{\sqrt{|\bar{k}|}}\,\bar{K}(\omega, \bar{k}, T, L) \rightarrow I_{(s)i}$$

$$L^{3/2}\sqrt{|\bar{k}|}\;\bar{E}(\omega, \bar{k}, T, L) \rightarrow V_i \tag{9}$$

$$-jL^{3/2}\frac{\bar{k}\times\bar{H}(\omega, \bar{k}, T, L)}{\sqrt{k}} \rightarrow I_i$$

with i = x, y, z. Using this notation, for each "mode," $\bar{k}$, we may write two matrix equations that follow directly from Eqs. 7 and 8:

$$V_i = -Z_{ij}I_j \tag{10}$$

$$I_i = j\omega CV_i + Y_{ij}V_j + I_{(s)i} \tag{11}$$

The "voltages" and "currents" incorporating the three spatial components of the electric and magnetic fields have been normalized so that, for example,

$$\frac{1}{2}C\overline{|V_x|^2} = \frac{1}{2}\epsilon_o\overline{E_x(\omega, \bar{k}, T, L)\;E_x^*(\omega, \bar{k}, T, L)}\;L^3 \tag{12}$$

gives the energy storage of the x-component of the electric field of the mode $\bar{k}$ at the frequency ω and within the frequency interval $\Delta\omega$. A corresponding relation exists for all other energy storages. Similarly, for $\bar{K} = I_{si} = 0$,

$$\frac{1}{2}\overline{\left(V_iI_i^* + I_iV_i^*\right)} = \frac{1}{2}\overline{V_i\left(Y_{ij} + Y_{ji}^*\right)V_j^*} = \left(\bar{E}^*\cdot\bar{\bar{D}}\cdot\bar{E} + \bar{E}\cdot\bar{\bar{D}}^*\cdot\bar{E}^*\right)L^3 \tag{13}$$

is the power dissipated in the mode $\bar{k}$. Equation 13 shows that for a dissipative medium the tensor

$$\bar{\bar{D}} + \bar{\bar{D}}^\dagger$$

is positive definite or semidefinite for all real values of ω and $\bar{k}$.

We may now use the equivalent circuit (Eqs. 10, 11) to obtain the statistical

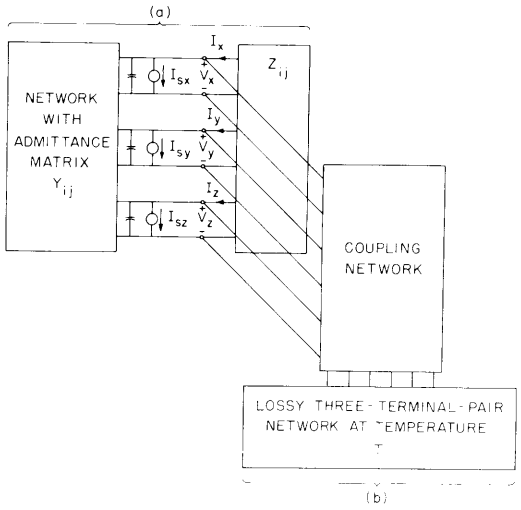

Fig. II-9. Coupling of cavity to electromagnetic system.

properties of $\overline{K}(\omega, \bar{k}, T, L)$.

If the cavity is at temperature T and coupled to another electromagnetic system at the same temperature, the power received by the cavity must equal the power emitted by it. In principle, any particular mode of the cavity could be coupled in a lossless manner with some other three terminal-pair network with the aid of an appropriately phased distribution of pickup antennas. Using the equivalent circuit for the excitation of the mode, we can represent the coupling scheme as shown in Fig. II-9. We can now borrow the results derived for linear circuits with thermal noise (2). The condition that there be no net power flow between the two three terminal-pair networks (a) and (b), of which network (b) has internal noise sources corresponding to a uniform temperature T of the network, will be met if, and only if, the noise current generators of network (a) satisfy the requirement (2)

$$\overline{I_{si}I_{sj}^*} = \kappa T \Delta f \left(Y_{ij}+Y_{ji}^*\right) \tag{14}$$

where κ is Boltzmann's constant. We use the letter T for temperature and for the period of the substitute process. Since the temperature always appears in conjunction with κ, no confusion should arise. (The impedance matrix Z_{ij} does not enter into expression 14 because of its lossless, anti-Hermitian character, $Z_{ij} = -Z_{ji}^*$.) Introducing the explicit expressions for I_{si} and Y_{ij} from the equivalent circuit for the cavity mode, we obtain

$$L^3 \overline{\overline{K}(\omega, \bar{k}, T, L)\, \overline{K}^*(\omega, \bar{k}, T, L)} = \left[\overline{\overline{D}}(\omega, \bar{k})+\overline{\overline{D}}^\dagger(\omega, \bar{k})\right] \kappa T \Delta f \tag{15}$$

where the dagger indicates the complex conjugate transpose of the tensor $\overline{\overline{D}}$.

Next, consider two different modes characterized by the propagation constants $\bar{k}$ and $\bar{k}'$. For each of these modes an equation of the form of Eq. 15 holds as a consequence of the network theoretical law (Eq. 14). A lossless coupling between these two modes results in the equivalent circuit of Fig. II-9. The net power transfer between the two networks will equal zero if and only if the noise sources of networks (a) and (b) are uncorrelated

$$L^3 \overline{K(\omega, \bar{k}, T, L)\, K^*(\omega, \bar{k}', T, L)} = 0 \qquad \bar{k} \neq \bar{k}' \tag{16}$$

Equations 15 and 16 yield, in the limit $T \to \infty$, $L \to \infty$, for the Fourier transform of the correlation function

$$\bar{\bar{S}}_K(\omega, \bar{k}) = \frac{\kappa T}{(2\pi)^4} \left[\bar{\bar{D}}(\omega, \bar{k}) + \bar{\bar{D}}^\dagger(\omega, \bar{k})\right] \tag{17}$$

(See ref. 4.) This law is a generalization of the Nyquist formula to distributed media.

The space-time correlation function is found from the inverse Fourier transform

$$\bar{\bar{R}}_K(\tau, \rho) = \frac{\kappa T}{(2\pi)^4} \int_{\bar{k}} \int_{\omega} \left[\bar{\bar{D}}(\omega, \bar{k}) + \bar{\bar{D}}^\dagger(\omega, \bar{k})\right] e^{j\omega\tau - j\bar{k}\rho}\, d\bar{k} d\omega \tag{18}$$

a. Application to an Electron Plasma

In a plasma in the absence of an applied dc magnetic field the field and driven-current density of the longitudinal plasma waves are related by the following relationship:

$$J_{dx}(\omega, \bar{k}) = DE_x = \left(j \frac{e}{m} \int \frac{u(\partial f_o/\partial u)}{(\omega - uk)}\, du \right) E_x \tag{19}$$

Since only the real part of D enters into the computation of the correlation function, we are interested only in Re(D) for real ω and k. Using the proper path and integration in the u-plane (5), as shown in Fig. II-10, we find that the only contribution to Re(D) comes from the integration around the semicircle:

$$\begin{aligned} \mathrm{Re}(D) &= \frac{e}{mk} \pi u \left.\frac{\partial f_o}{\partial u}\right|_{u=\omega/k} \\ &= \omega_p \epsilon_o \left(\frac{\pi}{2}\right)^{1/2} \frac{\omega^2}{\omega_p^2} \frac{1}{(ka)^3} \exp\left[-\frac{\omega^2}{2\omega_p^2 (ka)^2}\right] \qquad k > 0 \end{aligned} \tag{20}$$

with

$$\omega_p^2 = \frac{e^2}{m} \frac{n_o}{\epsilon_o}$$

and

$$a^2 = \frac{\kappa T}{m \omega p^2}$$

where a is the Debye radius.

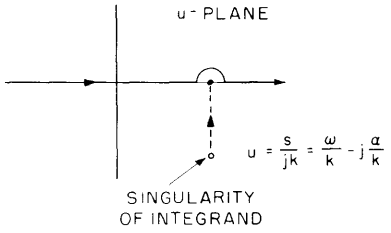

Fig. II-10. Integration path in u-plane for Eq. 4.

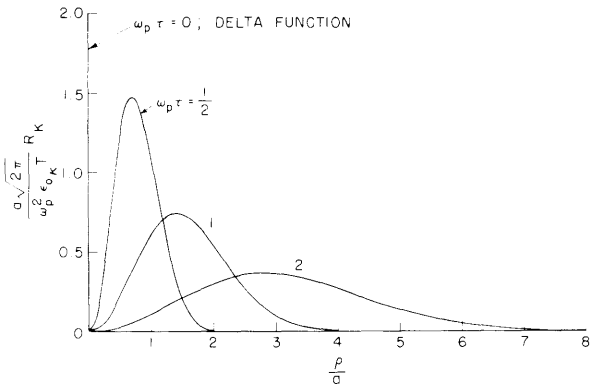

Fig. II-11. Plot of R_K versus ρ/a with $\omega_p\tau$ as parameters.

When $k < 0$, the path of integration in the u-plane has to be indented downward. We find that Re(D) is symmetric in k. Using Eq. 18 in one-dimension, we find

$$R_K(\tau, \rho) = \frac{e^2}{(2\pi)^{1/2}} \left(\frac{\kappa T}{m}\right)^{1/2} n_o \frac{m\rho^2}{\kappa T|\tau|^3} \exp\left(-\frac{1}{2}\frac{m\rho^2}{\kappa T\tau^2}\right) \tag{21a}$$

$$R_K(\tau, 0) = 2e^2\left(\frac{\kappa T}{m}\right)^{1/2} n_o \delta(\tau) \tag{21b}$$

and

$$R_K(0, \rho) = \frac{e^2}{m} \kappa T n_o \delta(\rho) \tag{21c}$$

Figure II-11 shows cuts through $R_K(\tau, \rho)$ at various values of $\omega_p\tau$ as a function of ρ/a. The maxima of the graphs in Fig. II-11 lie at $\rho_m = (2\kappa T/m)^{1/2}\tau$ and decrease inversely with τ. (Compare Eq. 21a.) The maxima of the crosscorrelation "move out at a speed" corresponding in order of magnitude to the thermal velocity of the electrons.

The self-correlation of $\overline{K}(t, \bar{r})$ is a delta function indicating a random excitation with very (ideally, infinitely) short relaxation time. Similarly, the crosscorrelation of $\overline{K}(t+\tau, \bar{r})$ and $K(t, \bar{r}')$ is zero for all values of $\bar{r} \neq \bar{r}'$ and $\tau = 0$. This means that the noise excitations at different points in the plasma are mutually correlated only after the time necessary for thermal electrons at $\bar{r}$ to have moved to $\bar{r}'$, and vice versa. The function $R_K(\tau, \rho)$ is proportional to the particle density n_o, and does not depend in any other way upon n_o. Since R_K can be ascribed to the random fluctuations of the particle density, its proportionality to n_o is a simple consequence of the Gaussian law of the mean-square deviation of a random number. Equation 21a does not change character with the density of the plasma and shows, therefore, that the same fluctuation laws that produce the

source current are applicable to dense, as well as to rarefied, plasmas. For the latter, however, it is not difficult to derive R_K from physical reasoning. It can be shown that the following form for the ensemble average of the density function perturbation f_1 is valid for a thin plasma:

$$uv\overline{f_1(t, x, u)\, f_1(t+\tau, x', v)}\, dudv = uf_o(u)\, \delta\left(\tau - \frac{x'-x}{u}\right) \delta(u-v)\, dudv \qquad (22)$$

with $\rho = x' - x$; and δ, the Dirac delta function.

Using Eq. 22 and noting that the source-current density K is given by $K = e\int uf_1(t, x, u)\, du$, we have for the correlation function, $\overline{K(t+\tau, x)\, K(t, x)}$, the result of Eqs. 21.

Thus the flucutation formulas (Eqs. 21) for a thin plasma can be derived from physical reasoning alone. It is the merit of the general relation (Eq. 18) that it yields a result that is correct for dense, as well as thin, plasmas.

H. A. Haus

References

1. S. M. Rytov, Theory of Electrical Fluctuations and Thermal Radiation (Izd-vo Akademiia Nauk S. S. S. R., Moscow, 1953).

2. H. A. Haus and R. B. Adler, Circuit Theory of Linear Noisy Networks (Technology Press of Massachusetts Institute of Technology, Cambridge, Mass., and John Wiley and Sons, Inc., New York, 1959).

3. N. Wax, Selected Papers on Noise and Stochastic Processes (Dover Publications, Inc., New York, 1954).

4. Compare the laws used here with their one-dimensional counterparts in W. B. Davenport and W. L. Root, An Introduction to the Theory of Random Signals and Noise (McGraw-Hill Publishing Company, New York, 1958).

5. L. Landau, Electron oscillations treated by the Laplace transform method, J. Phys. (U. S. S. R.) 10, 25 (1946).

2. HOLLOW-CATHODE DISCHARGE

The experimental study of the hollow-cathode discharge and its interaction with an injected electron beam continues. New equipment required for the continuation of experiments described in Quarterly Progress Report No. 58 (pages 35-41) is being designed and fabricated.

The interaction of the discharge and a pulsed electron beam injected along the discharge axis was observed over a wide range of discharge operating conditions. The method used for injection of the electron beam was previously described (1). Observations were made of the current pulse produced by beam electrons collected by the hollow

cathode. We observed that the magnitude of the current pulse is a function of the discharge parameters. The peak-to-peak magnitude was greatest when the discharge current and pressure were relatively low, and the magnitude decreased continually with increasing current or pressure until the pulse was no longer visible in the noise. We also observed the collected current pulse when no discharge was running, but the gas flow through the hollow cathode and the potential of the hollow cathode were the same as those that exist under discharge operating conditions. Some of the prominent characteristics of the current pulse wave shape under these conditions were also present in the current pulse observed when the discharge was running. In particular, the pulses have a negative peak, caused by charge flow that is opposite to the flow of the collected electrons, which takes several microseconds to decay. From this observation we concluded that the response to the injected electron beam is closely related to the dynamics of the hollow cathode itself, as well as to the dynamics of the electron-beam interaction with the discharge.

The effect of the discharge column on the reflection of microwave energy from the end of an open waveguide was studied with the use of the method previously described (1). The frequency range covered was 12.4-18 kmc. The discharge column passes approximately 1 cm from the open end of a rectangular waveguide. An electronically swept backward-wave oscillator was used as a signal source. Recordings were made, with and without the discharge running, of the output of a crystal detector mounted on an H-plane Tee. Comparisons made of the two recordings, which were obtained for a wide variety of discharge operating conditions, indicate that the oscillator frequency was always less than the plasma resonant frequency. Further experiments at higher frequencies, which will include measurement of transmission as well as reflection, are being planned.

A new vacuum chamber for the hollow-cathode discharge is under construction. A fivefold increase in pumping speed is expected because of rearrangement of the vacuum pump system. If operation of the discharge at lower pressures is possible, it is hoped that troublesome discharges occurring in the electron gun will be eliminated.

W. D. Getty, L. D. Smullin

References

1. W. D. Getty and L. D. Smullin, Experimental results of the study of the hollow-cathode discharge, Quarterly Progress Report No. 58, Research Laboratory of Electronics, M.I.T., July 15, 1960, pp. 35-41.

3. STUDIES OF THE HOLLOW-CATHODE DISCHARGE PLASMA

The hollow-cathode discharge plasma facility now in use is basically similar to that described in previous reports (1, 2). The experiments carried out during the last

quarterly period were mainly of an exploratory nature, and serve primarily to indicate promising avenues of research. However, enough detailed work has been carried out to enable us to describe and explain, in some detail, the properties of the external plasma column. The operational mechanism of the cathode itself remains in doubt, although several experiments have been devised and will soon be performed, which we hope will clarify this point. Our discussion is divided arbitrarily into several sections.

a. Cathode Variations

(i) High-current cathodes. The addition of tantalum radiating fins to a cathode tube with slightly thicker walls, for reduction of resistive heating, results in a significant increase in arc current capacity. One cathode configuration has been operated for short periods at 240 amp (>3000 amp/cm^2 at the orifice) with no sign of impending failure. Further trials will be performed when an adequate power supply becomes available. With an improved design of the radiating fins, a similar cathode was operated over the range 3-200 amp.

(ii) Large-diameter cathodes. Several sizes of tantalum tubing have been employed. The largest, thus far, is of 0.5-inch I.D. tubing. Operation was stable with a 0.5-inch diameter external plasma, 6 inches in length, for arc currents in excess of 90 amp. The external pressure at this current was approximately 2×10^{-3} mm. The instability at lower currents appears to be caused by conductive heat transfer to the cathode mounting. The operating temperature appears to be extraordinarily low, and further investigation of this point is planned.

(iii) Cathode material. Because tantalum undergoes a destructive reaction in a hydrogen atmosphere, several tungsten cathodes were constructed and used for the generation of a hydrogen-arc plasma. The region of stable operation of the hydrogen arc is smaller than the stable region for the other gases used and, for this reason, the bulk of the work discussed in this report refers to an argon-arc plasma.

b. Configuration Variations

(i) Gas flow and pressure. A study was made of the variation of electrical parameters with both gas flow and ambient pressure as independent variables. The pressure was varied from 10^{-4} to 5×10^{-3} mm Hg and flow from 0.1 to 3.0 cc-atm/sec. The results show a strong dependence of electrical properties of the arc upon ambient pressure, which has not yet been adequately explained.

(ii) Baffled reflex arc. A series of experiments was performed in which both the cathode and an annular anode were located at the same end of the magnetic-field region (see Fig. II-12). By control of the apertures of the three diffusion pumps, it is possible to control the relative pressures in the right-hand and left-hand regions. In particular, we found that the background pressure in the arc region may be reduced by at least a

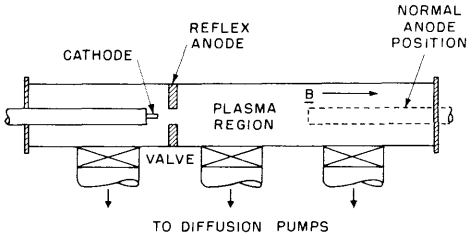

Fig. II-12. Experimental arrangement for reflex arc operation.

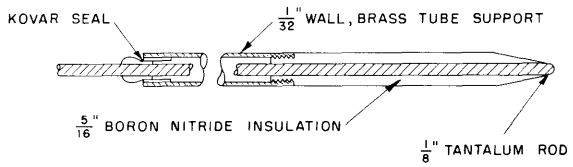

Fig. II-13. Probe detail.

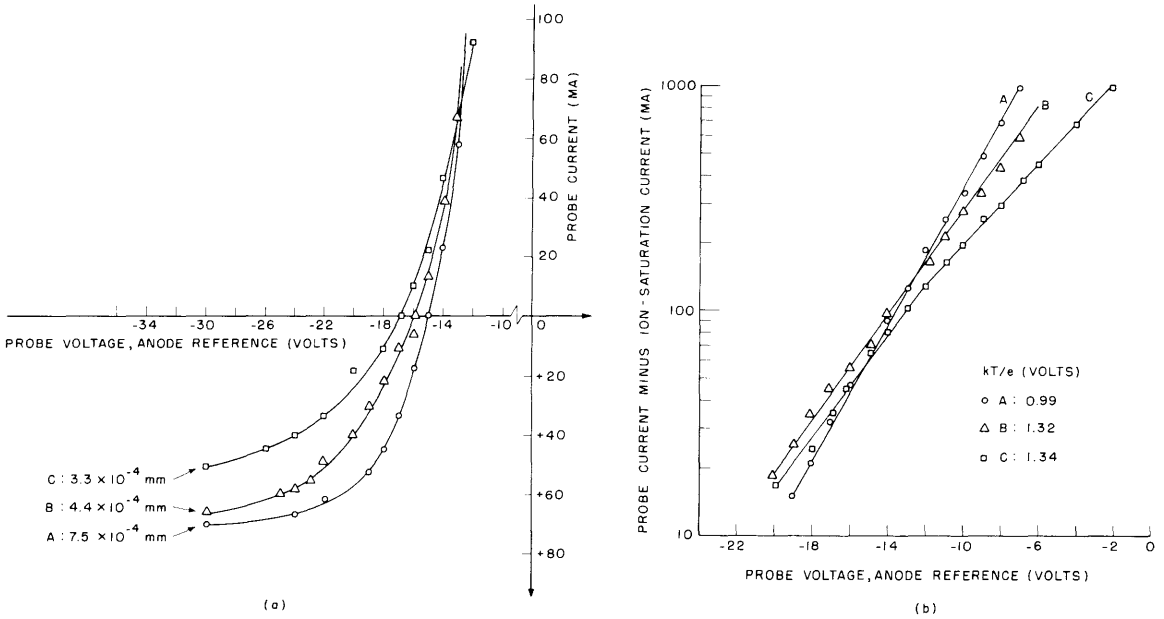

Fig. II-14. (a) Probe characteristics for several neutral argon gas pressures for reflex arc arrangement: arc current, approximately 20 amp; axial magnetic field, approximately 400 gauss; background argon pressure for each measurement is indicated on curves. (b) Semilogarithmic plot of data presented in (a). Temperatures for each case were determined from simple probe theory.

factor of 3 by throttling the left-hand pump (Fig. II-12) while reducing the gas flow rate.

c. Preliminary Diagnostics

(i) Probes. The plasma energy and density attained in the operation of the hollow-cathode discharge plasma are such that application of the standard "nonperturbing" analytic techniques is rendered quite difficult. Because of this, recourse was had to the use of ordinary Langmuir probes (see Fig. II-13). The comparatively large size is used for several reasons: (a) The probe is large compared with the electron Larmor radius

and small compared with that of the ions. This leads to some simplification of interpretation. (b) A large heat capacity and conductivity are necessary because of the high plasma density. (c) The edge effect is rendered reasonably small.

Pulsed techniques were ruled out, at least for the present, because of the very high noise level at several kilocycles.

A set of probe curves for slightly differing ambient pressures is presented in Fig. II-14a and -14b. A plasma temperature of approximately 1 volt and density of approximately 5×10^{12}, as shown in the curves, is quite representative of the normal operating range.

The shape of the probe curve is strongly dependent upon the orientation of the probe face with respect to the magnetic-field lines. For a probe perpendicular to the main B_z field, it is found that the ratio of electron-to-ion saturation currents is in the range 10-100, whereas classical probe theory predicts a value of at least $(m_i/m_e)^{1/2} \approx 280$ for argon. This is accounted for by the fact that electrons are hindered in their motion across field lines, and only those in the flux tube intersecting the probe face are drawn by the probe. This tube is quickly drained, and the electron current drawn is then more accurately a measure of diffusion into the flux tube than it is of local electron density. The ion saturation current, because of its small magnitude and because the ions may, to first order, be considered unaffected by the fields used, is indicative of the local density. This affords a convenient measure of plasma density variation within the apparatus and may, with the assumption of equal ion and electron temperature, be converted to absolute density. This is a conservative assumption in the density because it is extremely unlikely that the ion temperature exceeds that of the electrons.

Several other points are apparent from inspection of the curves. The electron current curve is quite accurately logarithmic. Comparison of charge density to the neutral density, as shown by the background pressure, indicates fractional ionization greater than 25 per cent at 20 amp.

(ii) Noise measurements. The noise signals imposed on both biased and floating probes were investigated for the frequency range from dc to approximately 1 mc. Although results, thus far, are inconclusive and somewhat nonreproducible, it appears that a strong signal with a frequency of 500 cps-10 kc is usually present. It is believed that this is caused by $\vec{E} \times \vec{B}$ rotation about the axis of the discharge, an effect similar to that observed by Nedeigh (3).

The discharge appears, under some conditions, to have two stable modes of operation, as indicated by sharp (approximately 50 per cent) changes in probe saturation current and noise level. This is similar to the observations of Lehnart (4), although in one case the change is discontinuous.

A probe situated at one side of the arc will show a dip (approximately 10 per cent) in ion saturation current if a probe placed diametrically opposite is driven at

approximately 900 cps. This may be ascribed to a sound wave in the sense of Alfvèn (5).

d. Other Observations

(i) Pulsed arc experiments. Pulsing of the arc current to significantly higher values than normal by discharge of a capacitor bank through the operating arc appears to be a very useful technique and several trials of this technique have been performed. It is interesting to note that the decay of the capacitive charge is given quite accurately by using the value of plasma resistance as given by Spitzer (6) and taking T = 10, 000°K. This is obviously fortuitous because the presence of sheaths and primary (high-energy) electrons obviates the applicability of simple theory.

(ii) "Short-circuited" field lines. Generally, field lines intersect the glass tube and therefore are not short-circuited in the sense of Simon (6). For this case, the ion saturation current at the walls is approximately 5 ma for the nominal probe size. If a grounded metal shorting plate is used, the ion saturation current drops to 0. 3 ma at the same position. The variation of transverse diffusion with differing return current paths is seen to be a quite pronounced effect.

e. Discussion

The values of plasma energy and density as measured by probes (1 ev, 5×10^{12} cm^{-3}) are corroborated by several other measurements: microwave measurements by Getty (7) that show the plasma to be opaque up to 17 kmc; estimates based on current density in the visible beam; spectrographic studies (2); and the observation that the floating potential is most negative at the center of the beam, and increases monotonically toward the walls (8). Comparison of these figures with the neutral-particle density at the operating pressures directly indicates that the fractional ionization is at least 25 per cent for arc current of 20 amp. At 1 ev the coulomb cross section (approximately 6×10^{4} $angstrom^{2}$) so greatly exceeds the neutral scattering cross section (<10 $angstrom^{2}$) that there can be no doubt that the plasma behavior is determined by electrostatic interactions; that is, we have a "highly ionized plasma."

Calculation of the Larmor radii of the confined particles indicates that the plasma generated is subject to hybrid confinement with magnetic confinement of the electrons and electrostatic confinement of the ions. This is further borne out by the observation of floating-potential variation.

f. Work in Progress

Several types of more sophisticated probe techniques (multipole, magnetic, and capacitive) are either planned or in use. Arc pulsing techniques are being refined and

give promise of achieving virtually 100 per cent ionization. The geometry of the system is particularly amenable to analysis and an intensive study of diffusion and resistivity in a transverse magnetic field will be carried out.

L. M. Lidsky, S. D. Rothleder, S. Yoshikawa

References

1. W. D. Getty, A low-pressure gas-arc device, Quarterly Progress Report No. 57, Research Laboratory of Electronics, M.I.T., April 15, 1960, pp. 27-29.

2. D. J. Rose, L. M. Lidsky, S. D. Rothleder, and S. Yoshikawa, Experimental results on the hollow-cathode discharge, Quarterly Progress Report No. 58, Research Laboratory of Electronics, M.I.T., July 15, 1960, pp. 41-44.

3. R. V. Nedeigh, Effect of pressure gradient on a magnetically columnated arc, Proc. Second International Conference on the Peaceful Uses of Atomic Energy, Geneva, September 1958, Vol. 31, p. 315.

4. B. Lehnart, Positive column in a longitudinal magnetic field, Proc. Second International Conference on the Peaceful Uses of Atomic Energy, Geneva, September 1958, Vol. 32, p. 349; F. C. Hoh and B. Lehnart, Phys. Fluids 3, 600 (1960).

5. H. Alfvèn, Phys. Fluids 3, 606 (1960).

6. A. Simon, Diffusion of arc plasma across a magnetic field, Proc. Second International Conference on the Peaceful Uses of Atomic Energy, Geneva, September 1958, Vol. 32, p. 343.

7. W. D. Getty, Research Laboratory of Electronics, M.I.T. (personal communication, May 1960).

8. Oak Ridge National Laboratory Semiannual Report, Oak Ridge, Tennessee, June 1960.

4. SUPERCONDUCTING SOLENOIDS – EFFECTS OF MAGNETIC FIELDS AND CURRENTS ON THE SUPERCONDUCTING TRANSITION

Small superconducting solenoids made of niobium (columbium) wire have been reported to generate magnetic fields up to 8 kilogauss (1, 2). The development of a large-volume solenoid for use in plasma research (3, 4) is the main objective of this work. The usefulness of such a solenoid would be greatly increased if it is capable of generating stronger magnetic fields. Therefore an investigation of the dependence of the superconducting-to-normal transition in niobium upon magnetic field, current temperature, treatment of the material, and other factors was started.

The first studies were made on niobium wire. Some of the wire was annealed by the manufacturer after the final drawing; in other samples this final anneal was omitted. It is apparent from published reports that the critical field of niobium varies greatly (values up to 12 kilogauss at 1.5°K have been reported (5)) and depends upon the heat treatment of the material and other factors (1, 5, 6).

The arrangement of the experiment is shown in Fig. II-15. The sample wire,

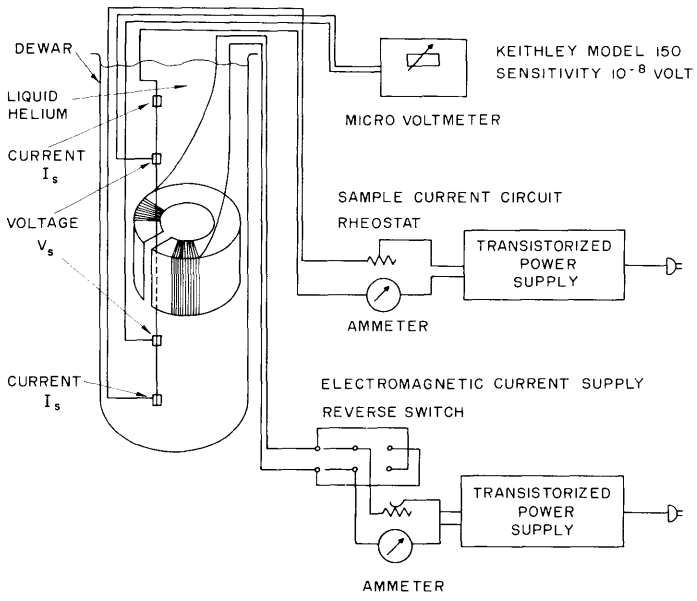

Fig. II-15. Schematic view of the experimental arrangement for the study of magnetic field-current relationship.

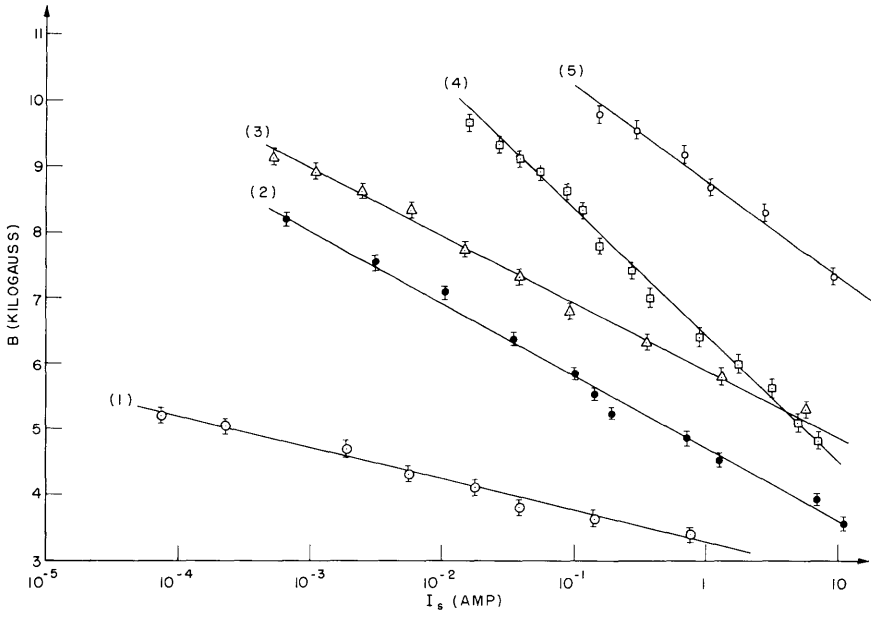

Fig. II-16. Magnetic field versus current for constant V_s (10^{-8} volt).

(1) Annealed wire (5AS-1), 0.005 inch, 4.2°K.
(2) Unannealed wire (7US-1), 0.007 inch, 4.2°K.
(3) Unannealed wire (4UN-1), 0.004 inch, 4.2°K.
(4) Unannealed wire (4US-2), 0.004 inch, 1.67°K.
(5) Unannealed wire (4UN-1), 0.004 inch, 1.56°K.

provided with current and voltage leads, is inserted into the gap of a small iron-core superconducting electromagnet (1) where it is exposed to a transverse magnetic field. The entire device is immersed in liquid helium either at atmospheric pressure (4.2°K) or at a reduced pressure as low as 4 mm (1.6°K).

The procedure adopted was to set the magnetic field, and then increase the sample current, I_s, until a voltage, V_s, can just be observed across the voltage leads. The current is increased again, and V_s versus I_s is measured. The procedure is repeated at different magnetic fields, B.

Figure II-16 shows the B versus log I_s plot for the minimum detectable V_s (10^{-8} volt) for a number of samples. The B versus log I data are well approximated by straight lines in all cases; this fact indicates a relation of the form

$$I = I_o e^{-KB} \tag{1}$$

The values of I_o and K for our experiments are given in Table II-1 for two temperatures.

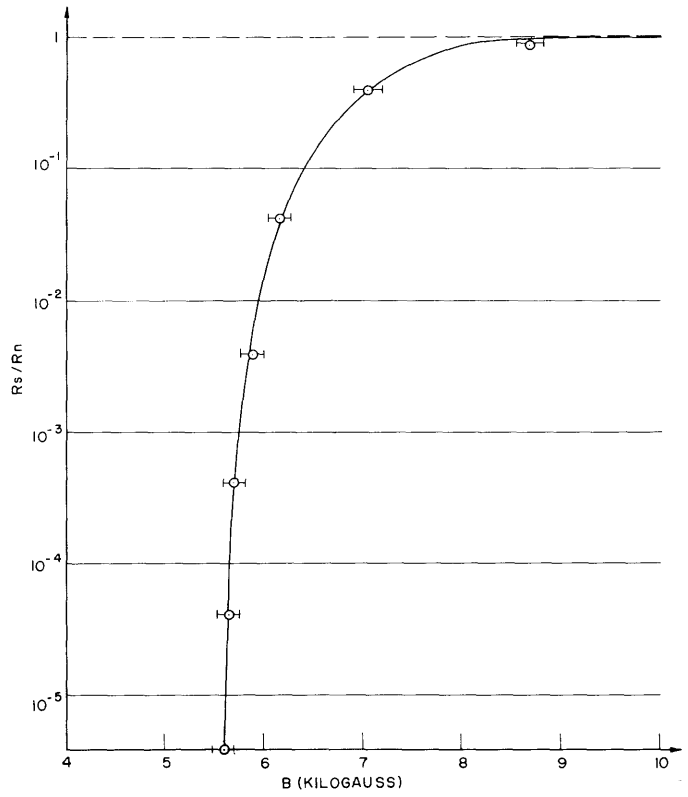

Fig. II-17. Relative resistance versus magnetic field at constant sample current. (I_s = 50 ma; sample 4US-7.)

Table II-1.

	4.2°K		1.6°K	
	I_o (amp)	K $(\text{kilogauss})^{-1}$	I_o (amp)	K $(\text{kilogauss})^{-1}$
Annealed wire	2.1×10^7	4.84		
Unannealed wire (7US-1, 4US-2)	1.49×10^4	2.04	1.2×10^3	1.11
Unannealed wire (4UN-1)	5.2×10^5	2.23	1.04×10^6	1.58

It is clear that the transition occurs at higher magnetic fields when the wire is unannealed, the temperature reduced, and the current reduced. Samples 7US-1 and 4UN-1 were made from different lots of unannealed wire from the same manufacturer. The reasons for the differences in their properties are not yet understood.

Figure II-17 shows a log R_s/R_n versus B plot at constant I_s, for a particular sample; $R_s = V_s/I_s$; and R_n is the value toward which the resistance tends as B becomes large. The value R_s was measured down to values as small as 10^{-5} R_n, and although it is a rapidly varying function of B, we could find no resistance discontinuity in any of the samples tested. The implication of this relationship for the design of magnets is that one should be able to reduce drastically the resistance of a solenoid by a slight reduction in the magnetic field that it generates.

It appears that with a practical limit of 0.1 amp current for 0.004-inch diameter niobium wire, fields in the vicinity of 10 kilogauss at 1.6°K may be feasible.

L. J. Donadieu, S. H. Autler

(S. H. Autler is a member of Group 82, Lincoln Laboratory, M.I.T.)

References

1. S. H. Autler, Rev. Sci. Instr. 31, 369 (1960).

2. S. H. Autler and D. B. Montgomery, Quarterly Progress Report on Solid State Research, Lincoln Laboratory, M.I.T., July 15, 1960, p. 63.

3. D. J. Rose, Bull. Am. Phys. Soc. 5, 367 (1960).

4. S. H. Autler, Bull. Am. Phys. Soc. 5, 367 (1960).

5. T. G. Berlincourt, Phys. Rev. 114, 969 (1959).

6. D. Shoenberg, Superconductivity (Cambridge University Press, London, 1960), p. 224.

II-C. PLASMA MAGNETOHYDRODYNAMICS AND ENERGY CONVERSION*

Prof. O. K. Mawardi
Prof. H. H. Woodson
Prof. J. A. Fay
Prof. W. D. Jackson
Prof. D. C. Pridmore-Brown
Prof. A. H. Shapiro
Dr. R. Gajewski†
T. I. Sundström
G. W. Bukow
L. Y. Cooper
R. S. Cooper
D. M. Dix
D. A. East
W. H. Heiser
G. B. Kliman
A. T. Lewis
J. K. Oddson
J. P. Penhune
E. S. Pierson
J. W. Poduska
K-F. Voyenli
B. Zauderer

1. THE MAGNETOHYDRODYNAMIC RAYLEIGH PROBLEM FOR THE NONCONDUCTING PLATE

a. Introduction

The classical Rayleigh problem can be extended to magnetohydrodynamics by considering the motion caused by the impulsive start, in a direction parallel to itself (the x-axis), of an infinite flat plate (the $y = 0$ plane) immersed in an infinite extent of an incompressible, viscous, electrically-conducting fluid initially at rest, with a magnetic field applied over space.

It is obvious that for the applied field parallel to the plate no electromagnetic effects are present, since no current is induced and consequently the Lorentz body force vanishes and hence no forces act on the fluid other than those expressed in the usual Navier-Stokes equations. However, for the applied field with a component perpendicular to the plate, there are induced currents and corresponding electromagnetic body forces. The problem is governed by the Navier-Stokes equations with the Lorentz force included, and Maxwell's equations. In general, the problem can be treated as four cases: the first two, for an infinitely conducting plate of either finite or infinitesimal thickness; the third, for a plate of finite thickness and conductivity; and the fourth, for a nonconducting plate of arbitrary thickness. These cases differ in boundary conditions, and the solutions for each are therefore decidedly different.

The basic problem considered here is that of the nonconducting plate with an applied field that is transverse to the plate and parallel to the +y axis. The problem is of interest because it gives insight into the general character of the flow to be expected in many practical applications, such as flow about obstacles and flow at nonconducting boundaries. This problem has been solved inadequately by Rossow (1, 2) and discussed inaccurately by Carrier and Greenspan (3).

---

*This work was supported in part by National Science Foundation under Grant G-9330; in part by Contract AF19(604)-4551 with Air Force Cambridge Research Center; and in part by WADD Contract AF33(616)-3984.

†Sloan Foreign Postdoctoral Fellow, from the Institute for Nuclear Research, Warsaw, Poland.

In Rossow's first solution, the assumption was made that the induced magnetic field is negligible. This assumption restricts the solution to the regime $\epsilon \equiv \sigma\mu\nu \ll 1$, and, although the numerical results are reliable in this regime, the solution completely suppresses the Alfvèn wave mechanism, and therefore does not provide a valid representation of the character of the flow. Rossow (2), in his second solution, lifts the restriction $\epsilon \ll 1$ and attempts to obtain the solution with two different sets of boundary conditions. However, neither set is compatible with a physically realizable situation, and the solution to his second case is incorrect. As we shall see, the primary difficulty is attributable to application of unrealistic boundary conditions.

Carrier and Greenspan began a treatment of the problem, but failed to carry it through because of a paradox observed in the general solution of the velocity profile in the limit as $t \to \infty$. They found that the velocity distribution in this limit is of the form $u = A + C \exp[-b(y)]$. Since they imply that this is a steady-state solution, they conclude that $\underline{E}$ must be nonzero because $\underline{J} = \sigma(\underline{E}+\underline{v}\times\underline{B})$ must certainly be zero as $y \to \infty$ in order for the induced field, that is, $\int_0^\infty J\,dy$, to be finite, and hence at $y \to \infty$, $\underline{E} = -\underline{v} \times \underline{B} = AB_{applied}$. They now observe that a finite $\underline{E}$ in steady state can only be due to a charge accumulation, and it is agreed that such an accumulation is quite artificial. This argument will be found invalid upon closer inspection of the meaning of the "steady-state" velocity distribution. Such a solution proposed by Carrier and Greenspan is valid as $t \to \infty$ only for $y \ll at$, where a is the Alfvèn velocity. It will be shown that an Alfvèn wave leaves the plate initially, and the implications of such a wave in an infinite space must produce a solution which, in fact, is never a steady-state solution. The general solution proposed by Carrier and Greenspan will be seen to be quite valid at $t \to \infty$, but only far behind the Alfvèn wave. With an understanding of the unsteadiness caused by the Alfvèn wave propagation the artificial charge accumulation is indeed seen to be nonexistent.

The solution for the problem of the infinitely conducting plate was obtained by Chang and Yen (4). They obtained exact solutions for a fluid with $\epsilon = 1$, and approximate solutions for other values of ϵ in which simplification of the equations could be made so that closed-form solutions might be extracted.

In view of these remarks, the purpose of this report is first, to obtain the solution to our nonconducting-plate problem, and second, to clear up some misconceptions that have been raised by other authors. Particular emphasis will be placed on the nature and number of boundary conditions to be employed.

b. Formulation of the Problem

Before proceeding to the formulation of the problem, it will be beneficial to give a qualitative physical picture. Initially, after the plate is set in motion, the motion of the

fluid induces a current in the positive z-direction. The Lorentz force is then acting to retard the fluid. However, the current tends to produce a longitudinal component of the magnetic field, which, in turn, produces an electric field that opposes the initial current. This induction is then responsible for the Alfvèn wave, which propagates and diffuses from the plate.

In the following analysis, fluid properties are considered constant and isotropic. The plate velocity is assumed to be much less than that of the speed of light, and the usual magnetohydrodynamic assumptions of neglecting the Maxwellian displacement currents and charge accumulation are made. The governing equations may be simplified by noting that since the plate is infinite in extent, no variable depends on either x or z. Then, from the continuity equation, $v^* = 0$, where the asterisk denotes a dimensionless variable. From the divergenceless properties of $\underline{B}^*$ and $\underline{E}^*$, we obtain $E_y^* = 0$, $B_y^* = B_o$, where B_o is the applied magnetic field. From $\nabla \cdot J = 0$, we have $J_y = 0$. The values of E_x^*, w^*, J_x^*, and B_z^* can be determined by investigating the initiating mechanism of the problem. As the plate is moved, a current J_z^* is induced. This current results in an induced B_x^* and consequently in the induced E_z^*. Since no further coupling of the equations exists, it is evident that the values of E_x^*, w^*, J_x^*, and B_z^* are no different from their initial values of zero. The variables in the problem are therefore reduced to u^*, B_x^*, J_z^*, and E_z^*, which are governed by the following equations:

$$\frac{\partial E_z^*}{\partial y^*} = -\frac{\partial B_x^*}{\partial t^*} \tag{1}$$

$$\mu J_z^* = -\frac{\partial B_x^*}{\partial y^*} \tag{2}$$

$$J_z^* = \sigma\left(E_z^* + u^* B_o^*\right) \tag{3}$$

$$\frac{\partial u^*}{\partial t^*} = \nu \frac{\partial^2 u^*}{\partial y^{*2}} - J_z^* \frac{B_o^*}{\rho} \tag{4}$$

(To be precise, the pressure is a fifth variable. However, it is given by the uncoupled equation $\partial p^*/\partial y^* = J_z^* B_x^*$ and will not be considered here.)

It is essential to examine Eqs. 1-4 at this stage, before any further reduction, to determine the number and nature of the boundary conditions. It is seen that one boundary condition is required on E_z^*, one boundary and one initial condition on B_x^*, and one initial and two boundary conditions on u^*. It is also permissible to substitute a boundary condition on J_z^* in place of the boundary condition on either (but not both) E_z^* or B_x^*. The boundary conditions for the present problem are

$$\left.\begin{array}{ll} E_z^* = 0 & \text{as } y^* \to \infty,\ t^* \geq 0 \\ B_x^* = 0 & \text{at } y^* > 0,\ t^* = 0 \\ B_x^* = 0 & \text{at } y^* = 0,\ t^* \geq 0 \\ u^* = 0 & \text{at } y^* > 0,\ t^* = 0 \\ u^* = U_o^* & \text{at } y^* = 0,\ t > 0 \\ u^* = 0 & \text{as } y^* \to \infty,\ t \geq 0 \end{array}\right\} \tag{5}$$

The first and last of these conditions arise from the fact that the motion of the plate is the initiating mechanism, and hence at distances far from the plate disturbances should diminish. The third condition arises from the symmetry of the problem and the fact that B_x^* must be continuous across the plate. That is, the lines of force must be symmetrical about the plate; furthermore, since B_x^* is continuous across the plate, the slope of the lines of force is also continuous; hence the lines of force are perpendicular to the plate at the plate and B_x^* equals zero.

The problem may now be formulated in more convenient terms by first introducing the following dimensionless variables: $B = B_x^*/B_o^*$, $u = u^*/a$, $y = y^* a/\nu$, $t = a^2 t^*/\nu$, $\epsilon = \sigma\mu\nu$, $U_o = U_o^*/a$, $J = J_z^* \nu\mu/B_o^* a$, $E - E_z^*/aB_o^*$. Eliminating J and E from Eqs. 1-4 yields

$$\left(\frac{\partial}{\partial t} - \frac{\partial^2}{\partial y^2}\right) u = \frac{\partial B}{\partial y} \tag{6}$$

$$\left(\frac{\partial}{\partial t} - \frac{1}{\epsilon}\frac{\partial^2}{\partial y^2}\right) B = \frac{\partial u}{\partial y} \tag{7}$$

Since this elimination involved differentiation of Eq. 3, the additional requirement that Eq. 3 must be satisfied at some boundary is necessary. If we select $y \to \infty$ as the appropriate boundary, the first of conditions 5 combined with Eq. 3 leads to the condition $\partial B/\partial y = 0$ as $y \to \infty$. This last condition and the last five conditions of Eqs. 5 are the appropriate boundary conditions for Eqs. 6 and 7. Finally, Eqs. 6 and 7 can be combined to yield:

$$\left\{\frac{\partial^4}{\partial y^4} - (1+\epsilon)\frac{\partial^3}{\partial y^2 \partial t} - \epsilon\frac{\partial^2}{\partial y^2} + \epsilon\frac{\partial^2}{\partial t^2}\right\}\left\{\begin{array}{c} u \\ B_x \end{array}\right\} = 0 \tag{8}$$

This equation, with the boundary conditions on B and u previously formulated, and the requirement that Eqs. 6 and 7 be satisfied, is the complete mathematical formulation of the problem.

c. Solutions and Discussion

(i) Solutions in Transformed Space

The problem is solved by using the method of Laplace transformation. The transforms of u and B are represented by $\bar{u}$ and $\bar{B}$, respectively. The solutions for $\bar{u}$ and $\bar{B}$ that satisfy the given boundary and initial conditions are

$$\bar{u} = \frac{\left(p-D_2^2\right) D_1}{\left(p-D_2^2\right) D_1 - \left(p-D_1^2\right) D_2} \frac{U}{p} \exp(D_1 y) + \frac{\left(p-D_1^2\right) D_2}{\left(p-D_1^2\right) D_2 - \left(p-D_2^2\right) D_1} \frac{U}{p} \exp(D_2 y) \tag{9}$$

$$\bar{B} = \frac{\left(p-D_2^2\right)\left(p-D_1^2\right)}{\left(p-D_2^2\right) D_1 - \left(p-D_1^2\right) D_2} \frac{U}{p} \exp(D_1 y) - \exp(D_2 y) \tag{10}$$

where D_1 and D_2 are given by

$$D_{1,2} = -\frac{1}{2}\left\{\left[\epsilon+(1+\epsilon+2\epsilon^{1/2})p\right]^{1/2} \pm \left[\epsilon+(1+\epsilon-2\epsilon^{1/2})p\right]^{1/2}\right\}$$

The general inversion of these equations for an exact solution involves an extremely large amount of manipulation; such solutions will not be dealt with here as they are not readily interpretable.

(ii) Exact Solution for $\epsilon = 1$

For this special case, the exact solution can be obtained with the aid of an inversion table (5). The solutions for u, B, and J are given by

$$\frac{u}{U_o} = \frac{1}{4}\left[1+\exp(y)\right] \operatorname{erfc}\left(\frac{y}{2t^{1/2}} + \frac{t^{1/2}}{2}\right) + \frac{1}{4}\left[1+\exp(-y)\right] \operatorname{erfc}\left(\frac{y}{2t^{1/2}} - \frac{t^{1/2}}{2}\right) \tag{11}$$

$$\frac{B}{U_o} = \frac{1}{4}\left[1-\exp(y)\right] \operatorname{erfc}\left(\frac{y}{2t^{1/2}} + \frac{t^{1/2}}{2}\right) - \frac{1}{4}\left[1-\exp(-y)\right] \operatorname{erfc}\left(\frac{y}{2t^{1/2}} - \frac{t^{1/2}}{2}\right) \tag{12}$$

$$\begin{aligned}\frac{J}{U_o} = {} & \frac{1}{4(\pi t)^{1/2}} \exp\left\{-\left(\frac{y}{2t^{1/2}} - \frac{t^{1/2}}{2}\right)^2\right\}\left[\exp(-y)-1\right] \\ & - \frac{1}{4(\pi t)^{1/2}} \exp\left\{-\left(\frac{y}{2t^{1/2}} - \frac{t^{1/2}}{2}\right)^2\right\}\left[\exp(-y)-1\right] \\ & + \frac{1}{4}\exp(y) \operatorname{erfc}\left(\frac{y}{2t^{1/2}} + \frac{t^{1/2}}{2}\right) + \frac{1}{4}\exp(-y) \operatorname{erfc}\left(\frac{y}{2t^{1/2}} - \frac{t^{1/2}}{2}\right)\end{aligned} \tag{13}$$

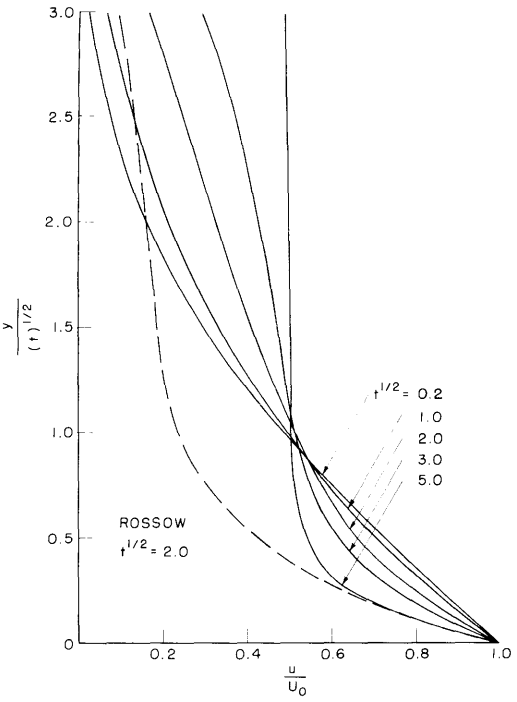

Fig. II-18. Velocity profiles for $\epsilon = 1$.

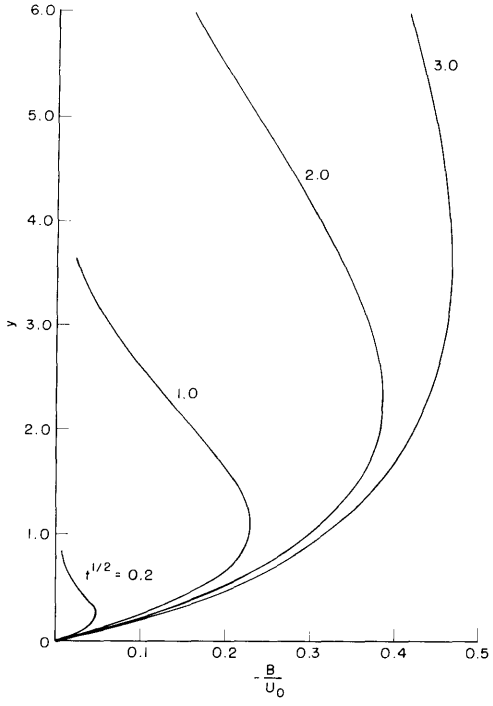

Fig. II-19. Magnetic field profiles for $\epsilon = 1$.

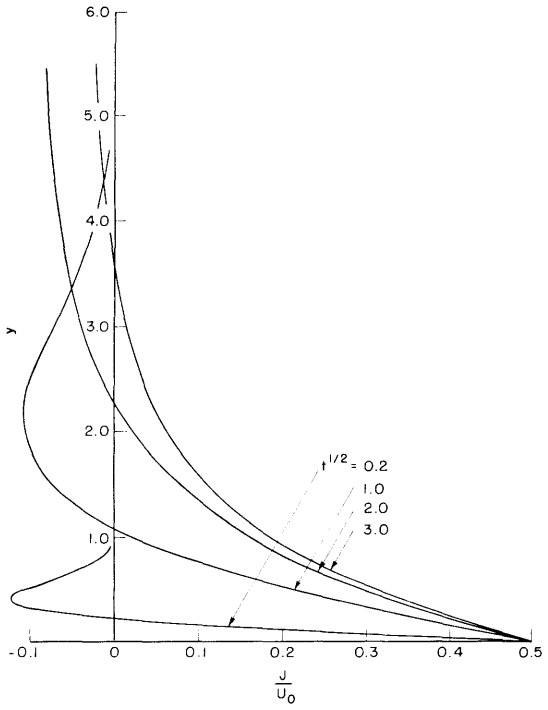

Fig. II-20. Current-density distribution for $\epsilon = 1$.

The solution for E can be obtained from Eq. 3, if desired.

These solutions for u, B, and J are plotted in Figs. II-18, II-19, and II-20. The physical phenomena portrayed by these solutions is described as follows. At t = 0, a viscous shear wave is generated by the motion of the plate. This shear wave, in turn, produces an Alfvèn wave (actually, a continuous succession of Alfvèn waves) and by this action is itself diminished. The eventual magnitudes of the two waves are dependent upon the ratio of the magnetic to viscous forces (ϵ) and are equal in this special case. The Alfvèn wave propagates at a velocity u = 1 and diffuses, while the viscous wave remains stationary and undergoes a finite diffusion that is limited by the electromagnetic forces that are not associated with the Alfvèn wave. Thus, at $t \gg 1$, when the Alfvèn wave is far from the plate, the velocity profile in the viscous layer next to the plate is time-independent (the thickness of the layer remains constant). These phenomena can be detected by observing the form of the solutions at various times. At $t \ll 1$ ($t^{1/2} = 0.2$, for example), the Alfvèn wave has not been fully generated, viscous forces predominate, and the solution differs but little from the classical Rayleigh solution. For $t \gg 1$, three regimes of flow are observed. For $y < t^{1/2}$, the viscous wave dominates, and has essentially reached its maximum amount of dispersion; the forces of inertia are zero. For $t^{1/2} < y \ll t$, the effect of diffusion of both waves is negligible, the region is current-free, and the resulting velocity is governed by the magnitude of the Alfvèn wave. In this special case, since the waves are of equal strength, the velocity is $U_o/2$. The adjacent region,

$y \approx t$, is dominated by the Alfvèn wave. For $y \gg t$, the effects of the diffusion of the Alfvèn wave are negligible, and the fluid is essentially undisturbed.

(iii) Solution as $t \to \infty$

This solution is obtained by allowing p to approach 0 in the transformed equations. The solutions for u and B are given by

$$\frac{u}{U_o} = (1+\epsilon^{1/2})^{-1} \exp(-\epsilon^{1/2}y) + \epsilon^{1/2}/1 + \epsilon^{1/2} \qquad y < t$$

$$\frac{u}{U_o} = (1+\epsilon^{1/2})^{-1} \exp(-\epsilon^{1/2}y) \qquad y > t \tag{14}$$

$$\frac{B}{U_o} = -\epsilon^{1/2}(1+\epsilon^{1/2})^{-1}[1-\exp(-\epsilon^{1/2}y)] \qquad y < t$$

$$\frac{B}{U_o} = \epsilon^{1/2}(1+\epsilon^{1/2})^{-1} \exp(-\epsilon^{1/2}y) \qquad y > t \tag{15}$$

It is observed that the change in velocity associated with the Alfvèn wave is given by $\epsilon^{1/2}/(1+\epsilon^{1/2})$. Unfortunately, the mathematical formalism involved completely suppresses the diffusion of the Alfvèn wave, and hence the solutions for $y > t$ are those to be attributed only to dispersion of the viscous wave.

(iv) Solution for $\epsilon \ll 1 (\sigma \to 0)$

This solution is for the case most often encountered in practice. By performing the appropriate limiting process, the solutions for u and B are found to be

$$\frac{u}{U_o} = \frac{1}{2} \exp(\epsilon^{1/2}y) \operatorname{erfc}\left[\frac{y}{2t^{1/2}} + (\epsilon t)^{1/2}\right] + \frac{1}{2} \exp(-\epsilon^{1/2}y) \operatorname{erfc}\left[\frac{y}{2t^{1/2}} - (\epsilon t)^{1/2}\right] \tag{16}$$

$$\frac{B}{U_o} = -\frac{\epsilon^{1/2}}{2}\left\{\exp(\epsilon^{1/2}y) \operatorname{erfc}\left[\frac{y}{2t^{1/2}} - (\epsilon t)^{1/2}\right]\right.$$

$$\left. - \exp(-\epsilon^{1/2}y) \operatorname{erfc}\left[\frac{y}{2t^{1/2}} + (\epsilon t)^{1/2}\right] - 2\operatorname{erf}(\epsilon t)^{1/2}\right\} \tag{17}$$

The solution for u is identical with that obtained by Rossow (1). It completely suppresses the Alfvèn wave, and hence the solutions will be accurate relatively close to the plate, but will not be accurate far from the plate, where the Alfvèn mechanism is dominant (however small) in any case.

The solution for $\epsilon \ll 1 (\nu \to 0)$ can also be obtained, but it necessitates a change in dimensionless variables and is of little practical interest; therefore it is omitted here.

d. Comparison of Our Solutions with Previous Work

Rossow (1, 2) selected two different sets of boundary conditions which he chose to distinguish by prescribing motion to the lines of force. The concept of prescribing motion to the lines of force is of dubious value in this problem and must be carefully applied to physical situations. This is demonstrated by his implication that moving the source of the magnetic field (located at infinity) will impart a uniform motion to the magnetic field and therefore alter the physical situation appreciably. It is obvious that if the plate is truly very far from the magnet, the disturbances caused by any motion of the magnet must be insignificant at the plate. Rossow's first case (the so-called field fixed-to-plate case) actually represents a situation in which at the same instant when the plate is set into motion a nonzero longitudinal component of the magnetic field is also prescribed. This situation is difficult to conceive on a physical basis and corresponds neither to the problem considered in this paper nor to the problem to which Rossow presumably addressed himself.

In reference to the boundary conditions employed by Rossow (6), it is evident that the initial conditions on $\partial u/\partial t$, J_z, and E_z are superfluous, while a necessary boundary condition on u has been omitted.

Rossow (2) implies that his second case is identical with the problem considered here. A representative solution for the $\epsilon = 1$ case is shown in Fig. II-18 for the purpose of comparison. The disagreement is severe and can be traced to the boundary condition on E. Rossow used the condition $E = 0$ at the plate, thereby implying that as $y \to \infty$, E is not zero. This contradicts the physical situation. Also, it is verified by direct substitution that the solutions for B and u proposed by Rossow do not satisfy the equation of motion (4).

D. M. Dix, L. Y. Cooper

References

1. V. J. Rossow, NACA Report 1358, 1958.

2. V. J. Rossow, Phys. Fluids 3, 395 (1960).

3. G. F. Carrier and H. Greenspan, J. Fluid Mech. 7, 22 (1960).

4. C. C. Chang and J. T. Yen, Phys. Fluids 2, 303 (1959).

5. G. A. Campbell and R. M. Foster, Fourier Integrals (D. Van Nostrand Company, Inc., New York, 1948).

6. V. J. Rossow, Phys. Fluids, op. cit.; see Table 1.

2. PLASMA MAGNETOHYDRODYNAMIC EXPERIMENTS

The objective of the present work on the magnetically driven shock tube is to study the phenomena that result from strong interaction between the plasma behind a shock front and a magnetic field. Strong interaction means that the gas flow strongly affects the magnetic field, which requires a high magnetic Reynolds number, and the magnetic field strongly affects the gas flow, which requires a high magnetic pressure.

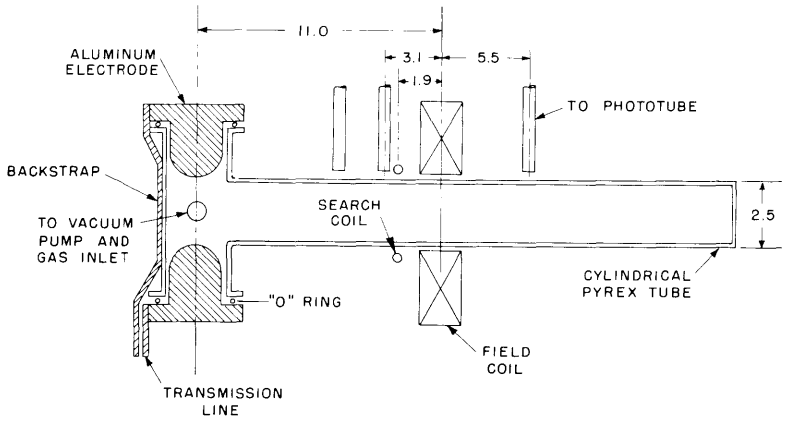

Fig. II-21. Sketch of shock tube showing details of construction and placement of field and search coils for experiment. (Dimensions in cm.)

After some minor modifications to the shock-tube equipment described in Quarterly Progress Report No. 51 (pages 28-30), attempts were made to obtain strong interactions. With the experimental arrangement of shock tube, field coil, search coil, and phototubes shown in Fig. II-21, measurements were first made at low magnetic-field strengths to determine the effect of the gas flow on the magnetic field. The results are shown graphically in Fig. II-22, in which the fractional flux change in the search coil is plotted as a function of the magnetic Reynolds number. The magnetic Reynolds number was calculated by using the conventional approach for calculating conductivity in a shock tube and with the tube radius used as a characteristic length. It is evident from Fig. II-22 that although a rather large magnetic Reynolds number is reached, the gas flow only moderately affects the magnetic field, changing it approximately 18 per cent for the best conditions achievable with the equipment. The curve of Fig. II-22 was taken with a maximum magnetic field of 1000 gauss. These results are similar to those obtained by Turner and Eastmond (1).

The conditions at the highest magnetic Reynolds number obtained, as shown in Fig. II-22, were chosen to try to change the gas flow by applying a magnetic field. The field coil was pulsed by a relay system from a 220-volt dc line to obtain fields as high as

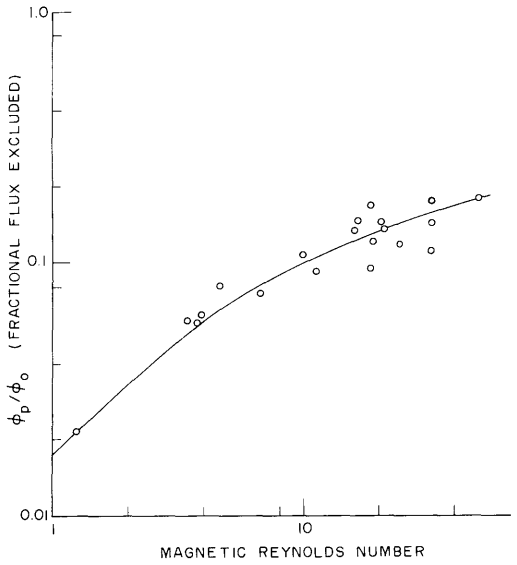

Fig. II-22. Fraction of flux excluded by a shock as a function of magnetic Reynolds number.

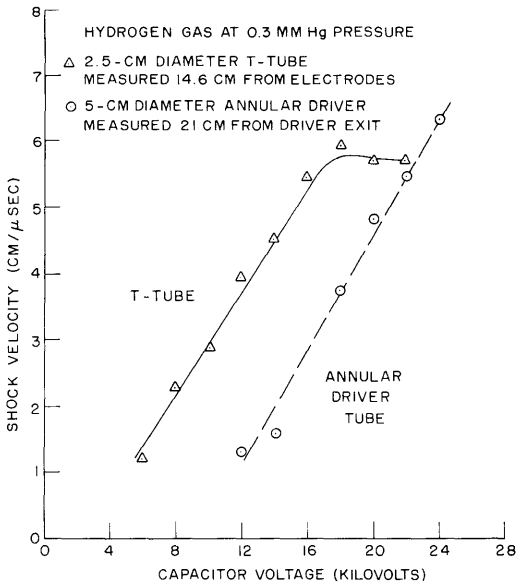

Fig. II-23. Shock velocity versus voltage for two types of shock tube.

6000 gauss. There were no measurable effects on the gas flow as indicated by the fractional flux change in the search coil, light output from the phototubes, or time of traversal of the gas through the field region. Order-of-magnitude calculations indicated that there should have been a measurable interaction.

The fact that there was no change in gas flow caused by the presence of the strong magnetic field may be the result of two effects. The magnetic Reynolds number may not be high enough to yield an appreciable field-free plasma for magnetic pressure to act on; or the magnetic pressure may not be high enough. Order-of-magnitude calculations indicate that either effect is equally likely, and so we decided to construct a shock tube to yield a higher magnetic Reynolds number.

In order to increase the magnetic Reynolds number, the velocity, characteristic length or conductivity (which depends strongly on velocity) must be increased. The plot of shock velocity versus voltage at constant pressure for the T-tube shown in Fig. II-23 shows that the obtainable velocity is definitely limited. This limitation appears to result from the decrease in driving effectiveness because the harder the tube is driven, the faster the initial shock leaves the discharge region. The T-tube is a very inefficient driver; less than 1 per cent of the energy stored in the capacitor bank is transferred to the gas behind the initial shock front. To improve the driving efficiency we decided to use an annular driver like Patrick's (2). With the expected increase in driving efficiency the shock-tube diameter was doubled. A drawing of the new shock tube with annular driver is shown schematically in Fig. II-24, and a plot of shock velocity versus

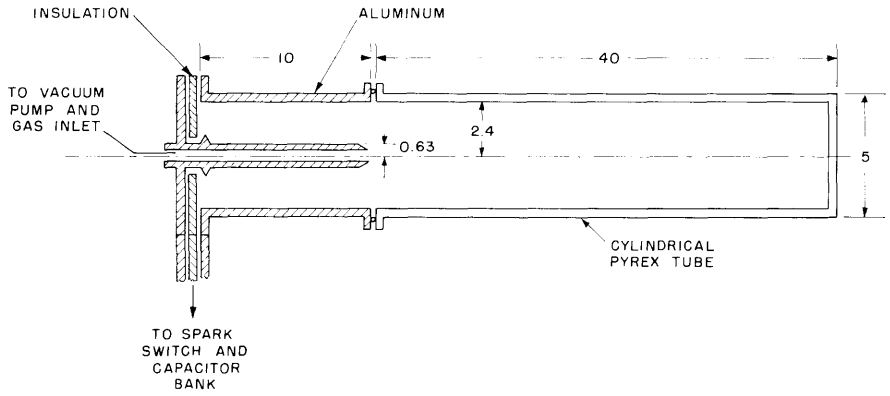

Fig. II-24. Schematic sketch of shock tube with annular driver. (Dimensions in cm.)

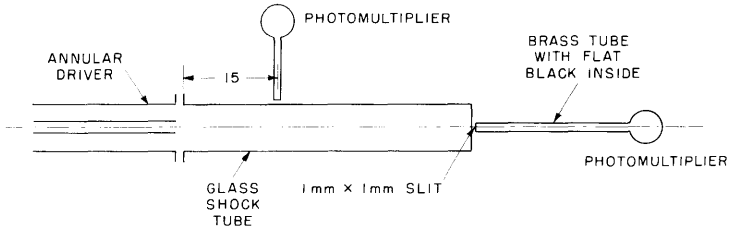

Fig. II-25. Experimental arrangement for viewing light output along the axis of shock tube.

voltage for a pressure of 0.3 mm Hg of hydrogen is shown in Fig. II-23. Comparison of the two curves in Fig. II-23 shows that, at least within the range of voltages used, the annular driver is much more effective than the T type of driver. Because the diameter of the new tube is doubled, at a given velocity the gas behind the shock front has more than four times as much energy as in the T-tube.

To properly perform the interaction experiments, a plane shock in the cylindrical tube is needed. The annular driver produces a toroidal-shaped shock wave that must form into a plane shock before experiments can be performed. Approximate theory indicates that after the shock wave has traveled a distance of approximately 3 tube diameters from the driver it should be plane. To verify this approximately the experiment shown schematically in Fig. II-25 was performed. The photomultiplier aimed along the axis of the shock tube was arranged to view a small cone no larger than the inner conductor of the annular driver. The photomultiplier placed 15 cm from the driver senses light across the shock-tube diameter. When a shock was produced with a capacitor voltage of 20 kv in hydrogen at 0.3 mm Hg pressure, the oscilloscope traces of Fig. II-26 were recorded. It is evident that light is present along the tube axis after the shock has traveled down the tube a distance of approximately 3 tube diameters. Thus, at distances greater that 15 cm

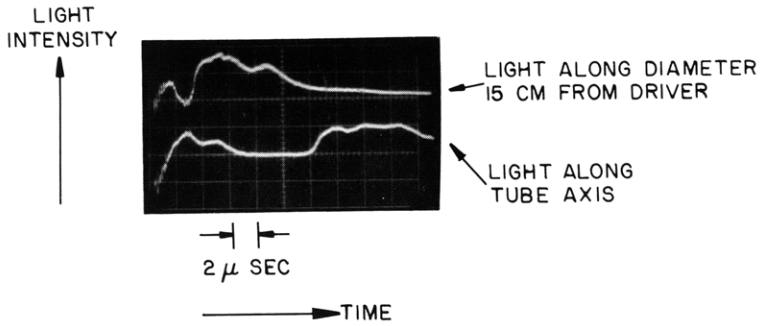

Fig. II-26. Light 15 cm from driver along the tube axis in hydrogen: pressure, 0.3 mm Hg; capacitor voltage, 20 kv.

from the driver, the shock front is approximately plane. In the oscilloscope trace of Fig. II-25 the increase in light intensity along the tube axis at 14 μsec is caused by the reflection of the shock wave from the end of the shock tube. Similar records of the photo-tube outputs at pressures higher than 0.3 mm Hg showed that the light reaches the tube axis in approximately the same time interval regardless of pressure, which indicates that for higher pressures the shock becomes plane in less distance than 3 tube diameters.

To obtain a measure of the improvement in magnetic Reynolds number and in the effect of the gas on the magnetic field with the new shock tube, the experimental arrangement of Fig. II-27 was used to obtain the data points shown in Fig. II-28 of fractional flux change in the search coil versus magnetic Reynolds number. The dashed curve in Fig. II-28 is taken from Fig. II-22 for comparison. It is evident that the plasma in the new shock tube affects the magnetic field more strongly than it did in the T-tube by a factor of approximately 40 per cent.

The data points in Fig. II-28 show that for high magnetic Reynolds numbers the fractional flux change decreases with increasing field and therefore the field appears to affect the gas flow. Probably this occurs because the ionized gas has not reached the center of the tube by the time the field region is reached. Figure II-26 shows that for a magnetic Reynolds number around 20 the ionized gas has certainly reached the center of the tube by the time the shock front reaches the magnetic field region; consequently, this point was chosen to make a measurement of fractional flux change as a function of magnetic flux density. The experimental arrangement of Fig. II-27 was used with a relay pulsing system for the field coil to obtain the data plotted in Fig. II-29. It is evident that the gas flow is affected by the magnetic field. At low field strengths the fractional flux change is independent of magnetic field strength, as it should be if the gas flow is unaffected. As the field strength is increased, the fractional flux change decreases, which indicates that the gas flow is probably being channeled by the magnetic field. Further evidence of channeling is the fact that at higher field strengths the traversal time of the shock front through the field region is decreased, and thus it appears that

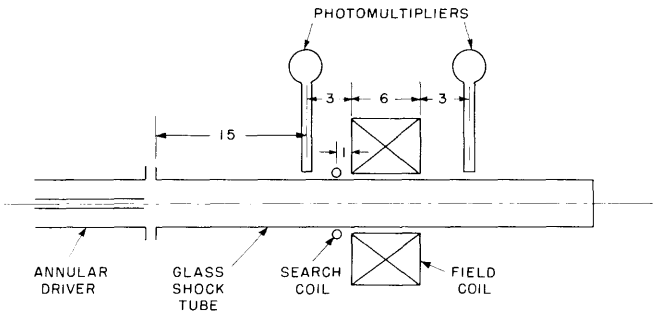

Fig. II-27. Experimental arrangement for interaction experiments with a 5-cm diameter shock tube having annular driver.

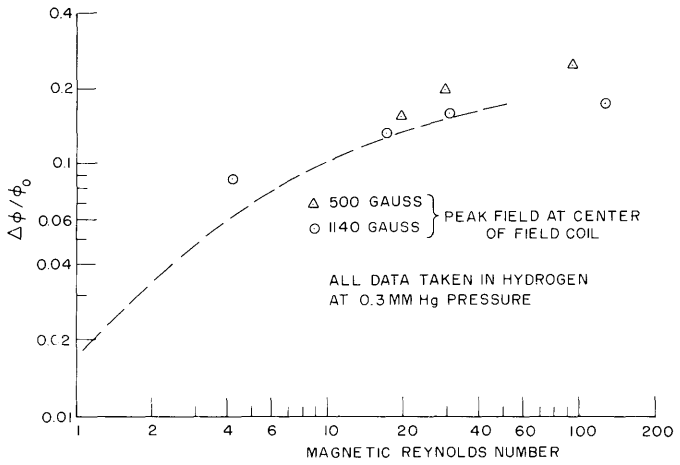

Fig. II-28. Fractional flux excluded in 5-cm diameter shock tube.

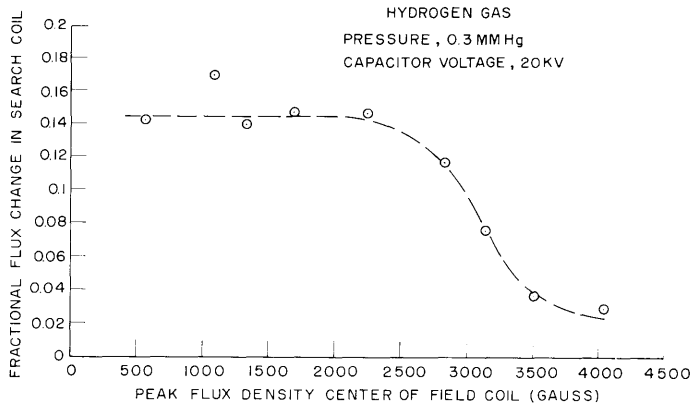

Fig. II-29. Fractional flux change in search coil as a function of flux density in 5-cm diameter shock tube.

the plasma is pushed away from the tube walls by the magnetic field and the drag on the gas caused by contact with the walls is reduced.

The experimental evidence presented indicates that the shock tube illustrated schematically in Fig. II-24, with its associated equipment, is an instrument in which the strong interaction between the ionized gas behind an almost adiabatically expanding shock front and a magnetic field can be made to occur. Thus the equipment can be used to study the detailed properties of the strong interaction.

H. H. Woodson, A. T. Lewis

References

1. E. B. Turner and E. J. Eastmond, Conductivity measurements of deuterium plasmas at magnetic Reynolds numbers greater than unity, Report GM-TR-0165-00514, Space Technology Laboratory, Los Angeles, California, December 1958.

2. R. M. Patrick, A description of a propulsion device which employs a magnetic field as the driving force, Report No. 28, AVCO Research Laboratory, Wilmington, Massachusetts, May 1958.